1957

Electronic specific heat of sodium tungsten bronze

Robert Wilson Vest
Iowa State College

NOTE TO USERS

ELECTRONIC SPECIFIC HEAT OF SODIUM TUNGSTEN BRONZE

by

Robert Wilson Vest

A Dissertation Submitted to the
Graduate Faculty in Partial Fulfillment of
The Requirements for the Degree of
DOCTOR OF PHILOSOPHY

Major Subject: Physical Chemistry

Approved:

Signature was redacted for privacy.

In Charge of Major Work

Signature was redacted for privacy.

Head of Major Department

Signature was redacted for privacy.

Dean of Graduate College

Iowa State College
1957

TABLE OF CONTENTS

ABSTRACT

The design and operation of a calorimeter for use in the temperature range 1.8-4.2°K. are presented, and the methods used in the treatment of data and calculation of results are discussed.

The heat capacities of several sodium tungsten bronzes (Na_xWO_3) were determined in the temperature interval 1.8-4.2°K. Samples having x equal to 0.89, 0.81, 0.73, 0.65 and 0.56 were studied. The measured heat capacities are described adequately by the sum of two terms, one linear and one cubic in temperature. The electronic specific heat of each sample is obtained by evaluating the coefficient of the linear term, and the Debye characteristic temperature derived from the coefficient of the cubic term.

Densities of one-electron energy levels at the Fermi energy, and effective electronic masses are calculated from the electronic specific heats. A plot of the density of states as a function of energy can be made if it is assumed that this curve is independent of sodium concentration. The justification of this assumption is discussed in the light of current theories of the solid state. The density of states curve rises rapidly at higher energies, and this rise is interpreted in terms of the filling of a Brillouin zone or of an overlap of two bands.

I. INTRODUCTION

The heat capacities of metals at very low temperatures ($<4^{\circ}K.$) are of interest for two reasons. The first is that the vibrational excitation of the lattice becomes more simple and clear cut since fewer spurious effects and complications enter. For example, the Debye approximation (1) and the more exact lattice theory of Born and von Karman (2) agree only at very low temperatures. The second reason for conducting calorimetry below $4^{\circ}K.$ is to study the contribution of the conduction electrons to the gross heat capacity of the metal. This electronic heat capacity is small compared to the total at all but the lowest temperatures.

The objective of this research was the determination of the heat capacity of sodium tungsten bronze (Na_xWO_3) as a function of sodium concentration. The temperature range of these experiments was $1.8\text{-}4.2^{\circ}K.$ The proposed measurements were of interest because the bronzes are unusual in the respect that sodium, and hence conduction electrons, can be added over a considerable range without affecting the crystallographic symmetry. This property insures that the Brillouin zone structure is the same for all of the cubic bronzes.

Measurement of the electronic specific heat of a metal will yield the density of one-electron energy states at one

value of energy, namely the Fermi energy. In the bronzes it is possible to vary the Fermi energy by varying the sodium concentration. Hence, an approximation of the density of states curve can be found for a portion of the energy spectrum, provided that the distribution of states is not appreciably modified by changing sodium concentration. Such information should be valuable in the interpretation and understanding of the electron theory of metals.

II. REVIEW OF LITERATURE

A. Sodium Tungsten Bronze

The sodium tungsten bronzes are non-stoichiometric sodium meta-tungstate, Na_xWO_3, where x varies from 0 to 1. At higher x (>0.3) the bronzes exhibit the typically metallic properties of luster and electronic conductivity. The color changes through blue, violet, red, and orange to yellow as x is increased from 0.3 to 0.9. The wavelength of the absorption maximum is a linear function of sodium concentration (3). The color can be qualitatively explained (3) on the basis of simple free electron theory.

The bronzes crystallize in the cubic perovskite structure (4) at all x greater than $\sim$0.3. Below x $\sim$0.3 the structure is tetragonal, and below x$\sim$0.15 a lower symmetry structure is obtained (5). Throughout the cubic range the lattice parameter is a linear function of sodium concentration (3), and this property permits a rapid analysis for sodium.

Two independent studies (6, 7) of electrical resistivity as a function of sodium concentration have shown a minimum near x = 0.75. The Hall coefficient (7) was found to vary inversely with the sodium concentration and to correspond to one free electron for each sodium atom in the crystal. The hypothesis of complete dissociation of sodium into positive ions and free electrons is further substantiated by magnetic susceptibility measurements (8, 9), which show that sodium

tungsten bronze is weakly paramagnetic. Thus, the resistivity minimum was attributed (7) to an anomalous maximum in the electron mobility. Gardner and Danielson (7) suggested the possibility of ordering of the sodium ions at x = 0.75 (three-fourths of the sites occupied) as an explanation of the mobility maximum, but thermal expansion measurements (10) cannot be interpreted in terms of an order-disorder transformation. Recent studies (11) of resistivity as a function of sodium concentration and anneal time have shown that the resistivity is a nearly linear function of sodium concentration at all temperatures after anneal.

Measurements of sodium diffusion (12) in sodium tungsten bronze yielded an activation energy considerably greater than that expected on the basis of simple vacancy diffusion and geometric considerations. An attempt (13) to interpret this high activation energy in terms of ionic bonding was quantitatively unsuccessful, but the calculations of total electrostatic energy as a function of sodium concentration did predict the correct stability range of cubic sodium tungsten bronze.

B. Helium Calorimetry

For the purpose of determining the heat capacities of metals at very low temperatures the calorimetric method of Nernst and Euken (14) has been almost universally used. In this procedure the sample is cooled to the desired tempera-

ture, thermally isolated from its surroundings, and the heat capacity determined by noting the temperature rises resulting from successive measured additions of energy. Most of the early calorimetry at liquid helium temperatures was conducted at the Leiden laboratory (15, 16). Later modifications (17, 18) of the design and techniques described by Keesom have not altered the basic method, but are concerned mainly with efforts to reduce the heat leakage, to develop better thermometers, and to improve the accuracy of the calculations.

The dynamical nature of calorimetry at liquid helium temperatures requires that a thermometer capable of yielding rapid temperature measurements be used. Resistance thermometers of leaded phosphor bronze (15), constantan (15), germanium and silicon semiconductors (19), carbon resistance cards (20), amorphous carbon (21), and carbon composition resistors (22) have been used with varying degrees of success. An ideal thermometer would have the characteristics: high temperature sensitivity, reproducibility, and insensitivity to measuring current and external fields. None of the thermometers developed to date combine all of these qualities to a completely satisfactory degree.

The resistance thermometers discussed above are all secondary thermometers and must be calibrated against a suitable standard. The International Temperature Scale of 1948 (23) is defined only to the oxygen point, and so no universally accepted scale exists in the liquid helium region.

In an effort to arrive at a common temperature scale in this low temperature region, members from cryogenic laboratories in the United States, Great Britain and Holland met in Amsterdam in 1948 and arrived at an "agreed" helium vapor pressure--temperature relation (24) based on the best experimental evidence available. During the 1955 Conference on Low Temperature Physics in Paris, the inadequacy of the 1948 liquid helium vapor pressure--temperature scale was discussed. The Conference members recommended that a p-T relation calculated by Dijk and Durieux (25) on a purely thermodynamic basis be adopted for a new agreed scale to replace the 1948 scale. As an alternative to the Dijk-Durieux calculation, a scale based on recent direct measurements of vapor pressure (26) was recommended. The use of this latter scale requires that vapor pressures be measured in certain specified ways.

C. Heat Capacity Theory

At sufficiently low temperatures, experiment has shown that the heat capacities of simple metals can be written as the sum of two terms, one linear and one cubic in temperature,

$$C = \gamma T + \beta T^3 \quad . \tag{1}$$

The term cubic in temperature is that due to vibrations of the constituent atoms about their equilibrium positions. A detailed explanation of this term requires a knowledge of the actual form of the vibrational spectrum of the solid. This problem is quite thoroughly treated in the recent book

by Born and Huang (27). The approximate theory of Debye (1) considers a crystal as an elastic continuum, and allows no frequencies greater than a maximum ν_m. Heat capacities calculated from this theory, after choosing ν_m to best fit experiment, are in close agreement with experiment despite the crude nature of some of the approximations made. Debye's theory predicts a T^3 temperature dependence of the lattice heat capacity at sufficiently low temperatures. The coefficient of this term is

$$\beta = 12/5\ \pi^4 nR(1/\theta_D)^3 \qquad (2)$$

where R is the gas constant, n is the number of atoms per formula weight in the crystal, and θ_D is the Debye characteristic temperature defined as $\theta_D = h\nu_m/k$, h and k being Plank's and Boltzmann's constants respectively.

The term linear in temperature in equation (1) arises from the electrons in the metal. The origin of such a term was first accounted for by Sommerfeld (29) by applying quantum statistics to an electron gas. If $g(\varepsilon)$ is the density of one-electron energy states per unit volume, then the total energy per unit volume E, and the electron density n are given by

$$E = n\bar{\varepsilon} = \int_0^\infty \varepsilon g(\varepsilon) f(\varepsilon) d\varepsilon, \qquad (3)$$

$$n = \int_0^\infty g(\varepsilon) f(\varepsilon)\, d\varepsilon \quad . \qquad (4)$$

Here $\bar{\varepsilon}$ is the average energy per electron, and $f(\varepsilon) =$

$1/(1 + \exp(\varepsilon - \varepsilon_F)/kT)$ is the Fermi-Dirac distribution function, ε_F being a normalizing factor commonly called the Fermi energy.

Defining two functions of energy $F(\varepsilon)$ and $G(\varepsilon)$ as

$$F(\varepsilon) = \int_0^{\varepsilon} \varepsilon g(\varepsilon) d\varepsilon \qquad G(\varepsilon) = \int_0^{\varepsilon} g(\varepsilon) d\varepsilon \quad ,$$

and calculating their first and second derivatives

$$F'(\varepsilon) = \varepsilon g(\varepsilon) \qquad G'(\varepsilon) = g(\varepsilon)$$

$$F''(\varepsilon) = g(\varepsilon) + \varepsilon g'(\varepsilon) \qquad G''(\varepsilon) = g'(\varepsilon)$$

reduces equations (3) and (4) to

$$(5) \quad E = \int_0^{\infty} F'(\varepsilon) f(\varepsilon) d\varepsilon$$

$$(6) \quad n = \int_0^{\infty} G'(\varepsilon) f(\varepsilon) d\varepsilon \quad .$$

It can be shown (30) for the case of $kT \ll \varepsilon_F$ that

$$\int_0^{\infty} F'(\varepsilon) f(\varepsilon) d\varepsilon = F(\varepsilon_F) + (\pi kT)^2 F''(\varepsilon)/6 \Big|_{\varepsilon=\varepsilon_F} + \ldots\ldots \quad .$$

Fourth and higher order terms are neglected. $F(\varepsilon)$ can be any function of energy. This reduces equations (5) and (6) to

$$(7) \quad E = F(\varepsilon_F) + (\pi kT)^2 F''(\varepsilon)/6 \Big|_{\varepsilon=\varepsilon_F} = \int_0^{\varepsilon_F} \varepsilon g(\varepsilon) d\varepsilon + (\pi kT)^2/6 \left[g(\varepsilon) + \varepsilon g'(\varepsilon) \right]_{\varepsilon=\varepsilon_F}$$

$$(8) \quad n = G(\varepsilon_F) + (\pi kT)^2 G''(\varepsilon)/6 \Big|_{\varepsilon=\varepsilon_F} = \int_0^{\infty} g(\varepsilon) d\varepsilon + (\pi kT)^2/6 \; g'(\varepsilon) \Big|_{\varepsilon=\varepsilon_F} \quad .$$

Differentiation of (7) with respect to temperature will

yield C_{el}, the electronic specific heat per unit volume,

$$(9)\quad C_{el} = \mathcal{E}_F\, g(\mathcal{E}_F)\, d\mathcal{E}_F/dT + \frac{\pi^2 k^2 T}{3}\left[\, g(\varepsilon) + \varepsilon g'(\varepsilon)\right]_{\varepsilon=\mathcal{E}_F} + \frac{(\pi kT)^2}{6}\left[2g'(\varepsilon) + \varepsilon g''(\varepsilon)\right]_{\varepsilon=\mathcal{E}_F}\left[\, d\mathcal{E}_F/dT\right] .$$

In order to evaluate $d\mathcal{E}_F/dT$, equation (8) is differentiated with respect to temperature, giving

$$dn/dT = 0 = g(\mathcal{E}_F)\, d\mathcal{E}_F/dT + \left[(\pi kT)^2 g''(\varepsilon)/6\right]_{\varepsilon=\mathcal{E}_F} d\mathcal{E}_F/dT + \pi^2 k^2 T g'(\varepsilon)/3\Big|_{\varepsilon=\mathcal{E}_F}$$

$$d\mathcal{E}_F/dT = -\pi^2 k^2 T g'(\varepsilon)/3 \left[\frac{1}{g(\varepsilon) + (\pi kT)^2 g''(\varepsilon)/6}\right]\Bigg|_{\varepsilon=\mathcal{E}_F} .$$

The second term in the denominator is small compared to the first and may be neglected. Substituting this result into equation (9) gives

$$(10a)\quad C_{el} = \pi^2 k^2 T g(\mathcal{E}_F)/3 + \pi^2 k^2 \varepsilon T g'(\varepsilon)/3\Big|_{\varepsilon=\mathcal{E}_F} - \pi^2 k^2 \varepsilon T g'(\varepsilon)/3\Big|_{\varepsilon=\mathcal{E}_F} + \text{higher order terms}$$

$$(10b)\quad C_{el} = \pi^2 k^2 T g(\mathcal{E}_F)/3$$

per unit volume, after neglecting the higher order terms. Multiplying equation (10b) by the molar volume will yield the electronic heat capacity per mole,

$$(11)\quad C_{el} = \pi^2 kRz\, g(\mathcal{E}_F) T/3n = \gamma T .$$

In this equation z is the number of conduction electrons per formula weight. This theoretical prediction of a linear dependence of electronic specific heat on temperature is con-

firmed by experiment.

By further assuming that the potential field acting on an electron in motion inside of a metal is a constant (simple free electron theory), the density of states is found to be (31) $g(\varepsilon) = C\varepsilon^{\frac{1}{2}}$ per unit volume, where

$$C = 4\pi(2m)^{3/2}/h^3 = (1/\varepsilon_F^\circ)\, 3n/2 \quad .$$

Here ε_F° is the Fermi energy at absolute zero. Equation (10b) then reduces to

(12) $$C_{el} = \pi^2 k^2 nT/2\ \varepsilon_F^\circ$$

per unit volume; or, per mole

(13) $$C_{el} = \pi^2 kzRT/2\,\varepsilon_F^\circ \quad .$$

It is assumed that $\varepsilon_F^\circ = \varepsilon_F$. Equation (12) is often referred to as the Sommerfeld equation.

From a quantum mechanical viewpoint, the use of the density of one-electron states demands that the total electronic wave function be composed of one-electron wave functions. The usual method of obtaining the total wave function is to use the Hartree approximation (32), which neglects all interactions between electrons. This is equivalent to the free electron gas approximation of Sommerfeld (29) in predicting electronic behavior.

It is known that electrons interact, but the extent to which this interaction controls their motion is not known. Exchange interactions can be taken into account by use of the Hartree-Fock approximation (33). However, this leads to a

temperature dependence in the specific heat not in accord with experiment (34, 35). Wigner (36) has suggested that Coulomb correlations will counteract the exchange correction, and so the qualitative agreement with experiment obtained with the simple Hartree expression is restored. Attempts to graft electron-phonon interactions (37) onto the independent electron model have proven unsuccessful in predicting the correct temperature dependence of the specific heat.

A quite different approach (38, 39, 40, 41) which emphasizes the collective correlated character of the electron motion, yields more consistant results. The correlated electron motion, corresponding to collective oscillations of the system as a whole, is considered at the outset of the theory. This model leads to the conclusion that the description of the electrons as a system of independent particles is often quite appropriate. This conclusion results because the effective interaction between electrons turns out to be a screened Coulomb law of force with a range approximately equal to the inter-electronic spacings. Thus, it is physically plausable to treat the electron system as a group of almost independent particles once the long range correlations which lead to this screening have been taken into account. A linear temperature dependence of the electronic specific heat is predicted in agreement with experiment.

III. MATERIALS AND APPARATUS

A. Materials

1. Preparation of samples

There is no phase diagram available for the sodium tungsten bronzes. Consequently, most of the information concerning their preparation is qualitative in nature. The methods which have been successfully employed involve reduction of a sodium tungstate or sodium tungstate-tungsten (VI) oxide melt. Reducing agents which have been successfully used (3) include hydrogen, tin, zinc, iron, phosphorous, and tungsten metal. Electrolytic reduction has also been employed (3). Solid phase reduction with tungsten metal appears to give the most nearly stoichiometric reaction, and hence the most predictable composition of bronze. However, this method was not used in this investigation because of the possible introduction of free tungsten which has a very large electronic specific heat.

The samples for this study were prepared by cathodic reduction. A mixture of sodium tungstate and tungsten (VI) oxide in a porcelain crucible was fused, and electrolyzed at an e.m.f. of less than 1 volt. The electrodes were graphite (anode) and nichrome (cathode). It was found that bronzes having sodium concentrations between 0.56 and 0.92 could be grown by decreasing the WO_3 from 50 to 20 mole per cent. Attempts to grow bronzes having x less than 0.56 by

increasing the WO_3 to more than 50 mole per cent always resulted in blue needles which had tetragonal symmetry and x less than 0.3. The reason for this inability to obtain cubic bronzes below x = 0.56 is not understood. Attempts to increase x above 0.92 by using more than 80 mole per cent Na_2WO_4 always resulted in no crystal formation. This observation is also not understood. Cubic crystals measuring one centimeter or more on an edge were grown. The perfection obtained increased with decreasing current density.

After growth the bronzes were broken up into small pieces (10-60 mesh) and cleaned by successive treatment with boiling water, aqueous ammonia, concentrated HCl, and aqueous HF.

2. Analyses of samples

The mole fraction of sodium in the bronzes was obtained by an x-ray determination of the precision lattice parameter. It has been found by several investigators (3, 5, 42) that Vegard's law holds throughout the cubic range of the bronzes. The following linear relationship between lattice parameter and sodium concentration was used in this study.

$$a_o = 0.0820x + 3.7845$$

In this equation a_o is the precision lattice parameter in Angstroms and x is the mole fraction of sodium in the formula Na_xWO_3. Comparisonsof this equation with chemical analysis in this laboratory have indicated an accuracy of 0.02 in the

value of x.

A back reflection powder camera and nickel filtered copper radiation were used. Five $K\alpha_1$ and five $K\alpha_2$ reflections were obtained. The lattice parameters calculated from these ten reflections were plotted against the function $\frac{1}{2}(\cos^2\theta/\sin\theta + \cos^2\theta/\theta)$ suggested by Nelson and Riley (43). Geometrical and absorption errors are minimized by extrapolating the lattice parameters obtained from several reflections to a Bragg angle of 90°. For the bronzes (12) it has been found that plotting the lattice parameter against the Nelson-Riley function yields a more nearly linear extrapolation than plotting against $\cos^2\theta$.

B. Apparatus

1. Mechanical features

a. Calorimeter. The general design is indicated in Figure 1. The cryostat was suspended from a rectangular brass plate P (26"x8"x1/4") which in turn was firmly supported by wall brackets. The liquid helium was contained in the inner Pyrex dewar vessel (34" long and 4" I.D.) which had a ring seal 4 inches from the top. A vacuum tight seal was made between the inner dewar and cap C by means of a rubber gasket. The inner dewar rested in a spherically hollowed out balsa wood ring which was supported from plate P by three thin steel cables and springs attached to evenly spaced turnbuckles TB. The outer Pyrex dewar vessel (40" long and 7" I.D.) contained

liquid nitrogen and rested on a table which could be elevated and locked into position. Each dewar was strip-silvered so that the height of the liquid helium could be seen.

Two pumping systems designated as PS-1 and PS-2 are shown in Figure 1. The first was used to evacuate chamber CH. It was an all metal system and among its components were a Welch No. 1405 fore-pump, an H-2-P purifying diffusion pump (50 liters/sec at 1 micron), a cold cathode gage tube, and a connection to stopcock 2 of the glass manometric system. A side tube between the fore-pump and diffusion pump permitted connection to an external system such as a leak detector. The second pumping system served to reduce the pressure over the helium bath. This second pumping system was provided with a Fulton sylphon valve in the main line plus a needle valve and a Cartesian diver manostat MS in the by-pass line. Also provided was an atmospheric outlet, a mechanical pressure vacuum gage, and an inlet from the helium line. The pump was a Kinney Model DVD 8810 (110 cubic feet per minute at 1 atmosphere).

The cap assembly was comprised of a brass cap into which the inner dewar fitted, a monel tube which was anchored to the plate P, and a bronze T-fitting. The T-fitting was penetrated at the top by a one-half inch stainless steel tube which served both as an evacuation tube and suspension for the chamber CH. Extending upward from the cap was a brass tube which served as a guide for the refrigerant transfer

Figure 1. Helium calorimeter.

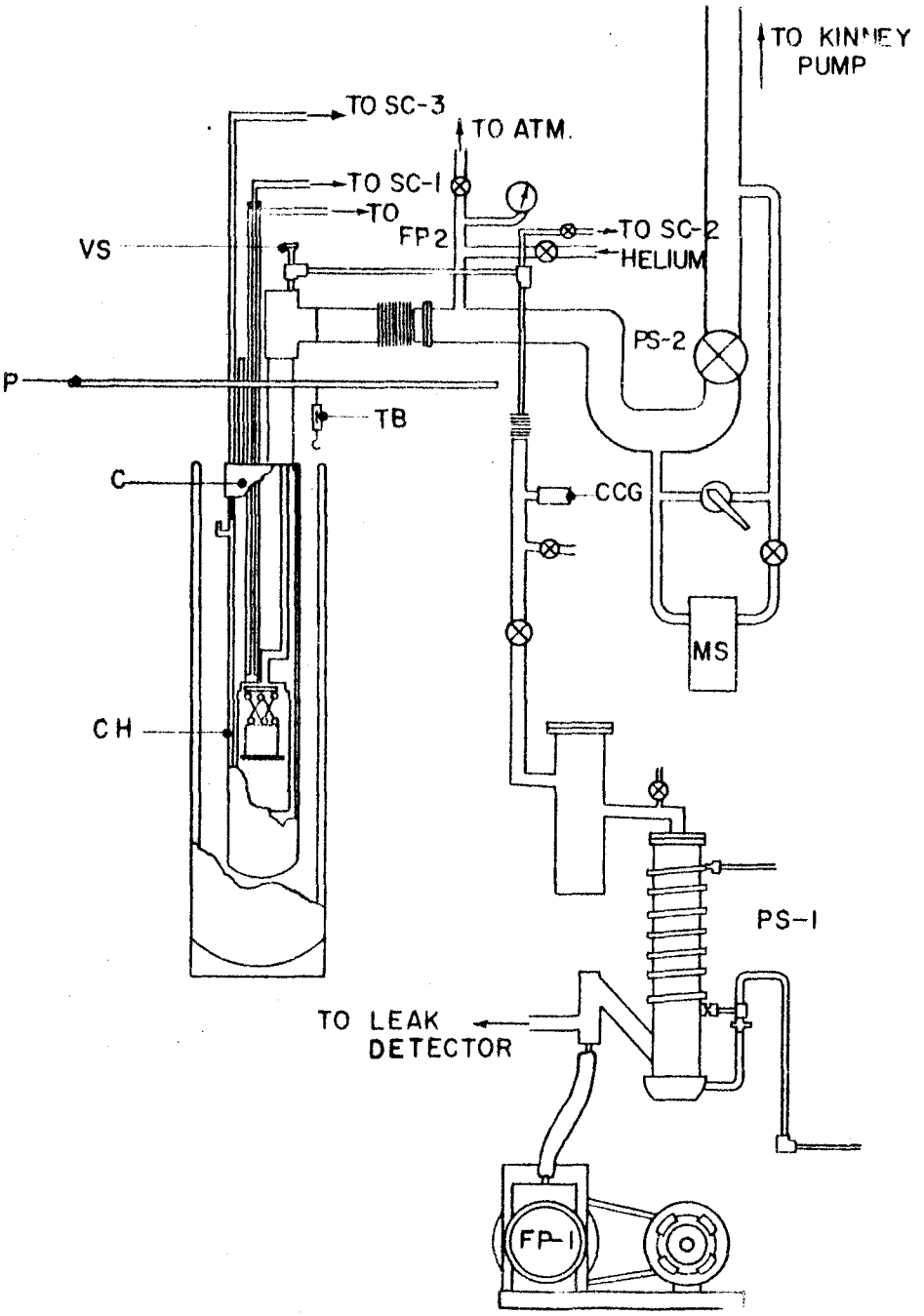
TO KINNEY PUMP
TO SC-3
TO ATM.
TO SC-1
TO FP2
TO SC-2
HELIUM
VS
PS-2
P
TB
C
CCG
MS
CH
PS-1
TO LEAK DETECTOR
FP-1

tube. This tube could be capped for operation under vacuum. Also penetrating the brass cap was a one-fourth inch copper tube extending upward to stopcock 3 of the glass manometric system, and a vacuum jacketed stainless steel vapor pressure thermometer which extended downward to the calorimeter chamber and upward to stopcock 1 of the glass manometric system. The off-center arrangement of tubes in the cap assembly permitted maximum use of the cap area. Below the cap, the stainless steel tube was brought back to center. The double elbow served as a radiation trap.

The calorimeter chamber (Figure 2) consisted of two parts: an upper cover which was permanently soldered to the stainless steel tube, and an outer can. The cover fitted into a concentric well at the top of the outer can and a vacuum tight seal was made with low melting indium solder. The bulb B of the vapor pressure thermometer was permanently soldered to the cover. A ring R around which electrical lead wires were wound was fastened by three 2-56 screws to tabs milled on the inside of the cover, and the gold plated sample can SC was suspended by fish line from three eyelets E on the bottom of this ring. A gold plated copper disc D was suspended between the eyelets and served as a radiation baffle. The sample can had a threaded well in the top for insertion of the resistance thermometer, and a heater wound on a thin copper ring HR connected to the well by radial fins F. The heater leads were brought out of the can through a

Figure 2. Calorimeter chamber.

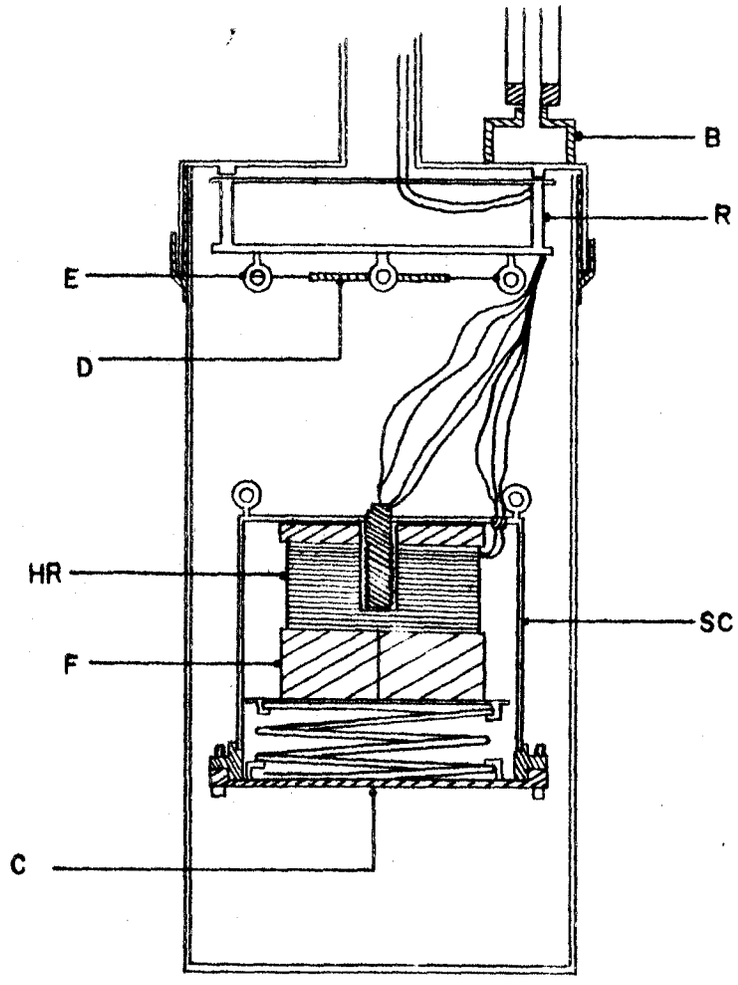
B
R
E
D
HR
SC
F
C

Stupakoff seal, and a spring loaded cap C was fastened to the bottom of the can by 2-56 brass screws.

b. Manometric system. The manometric system is shown in Figure 3. All of the glassware was mounted on a plywood panel (4'x5'x3/4"). The pressure of interest was introduced through SC-1 or SC-3 and measured with the mercury manometer MM, the oil manometer OM, or the McLeod gage MG. The mercury manometer was made of 14 mm precision bore tubing, and was illuminated by a fluorescent light behind the panel. The oil (Narcoil 20) manometer was made of 8 mm precision bore tubing.

The metering burette MB was used to introduce a known volume of gas to the vapor pressure thermometer under any desired pressure. It was provided with a mechanical pressure-vacuum gage and connections to the vapor pressure thermometer, the high pressure helium line, the manometric system proper, and fore-pump 2.

Helium exchange gas could be admitted to the calorimeter chamber through SC-2. The four-foot length of one-quarter inch copper tubing between SC-2 and the valve on the chamber pumping tube served as a metering volume for exchange gas. Kovar seals were used for all metal to glass connections.

2. Electrical features

The electrical leads were #40 double silk covered copper wire. The leads entered the cryostat through a vacuum seal

Figure 3. Manometric system.

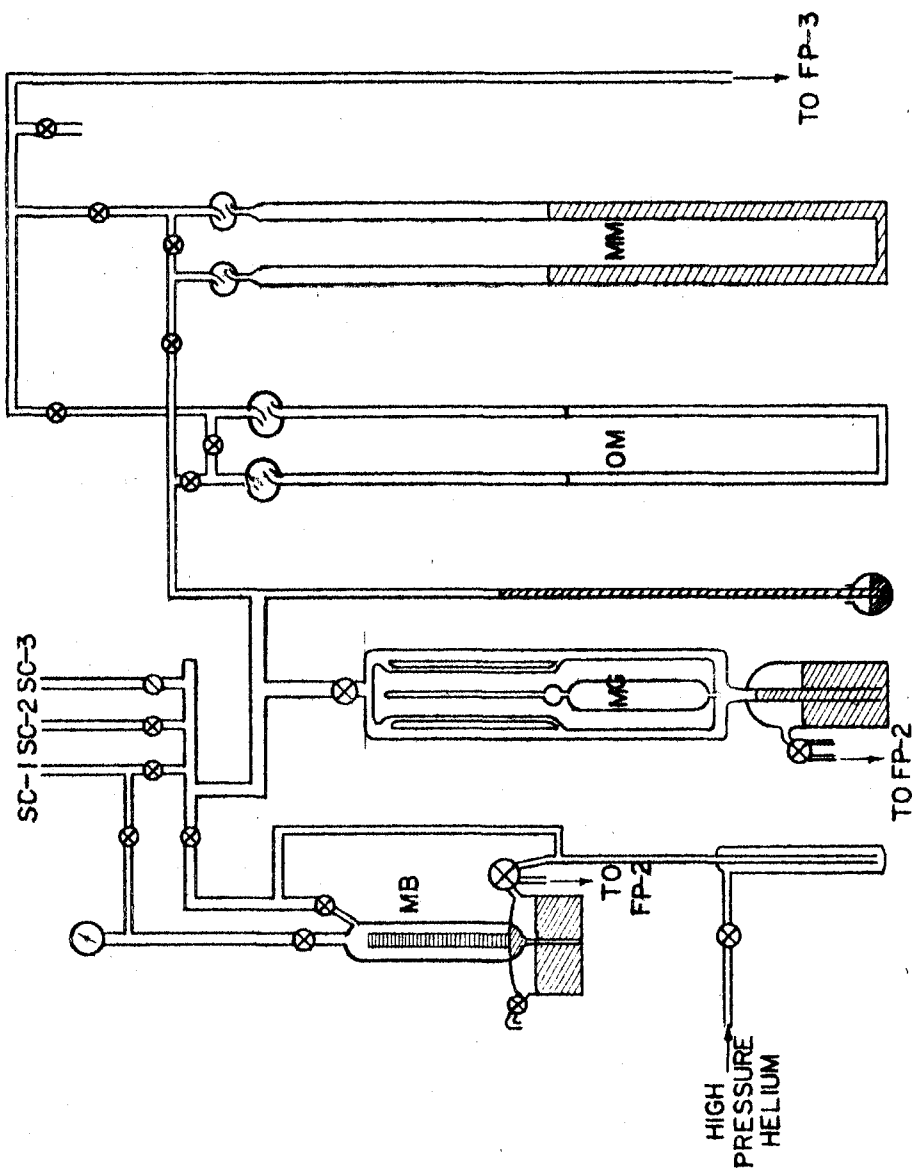
TO FP-3
MM
OM
MG
TO FP-2
SC-1 SC-2 SC-3
MB
TO FP-2
HIGH PRESSURE HELIUM

made by cementing them between a brass ring and a glass plate with Apiezon W. This vacuum seal VS (Figure 1) was in the room temperature part of the system, and was protected from mechanical damage by a cover. The lead wires were brought down the center of the stainless steel pumping tube and wound twice around the ring R (Figure 2), which had been covered with a layer of cigarette paper. The copper wires were then soldered to #40 manganin wires and the junctions brought in thermal contact with the ring by using G. E. adhesive. The manganin wires were wound twice around the ring before going to the sample can.

Two current and two potential leads went directly to the thermometer terminals. Two current leads and one potential lead went directly to the heater terminals on the top of the can. The other heater potential lead was joined to the current lead just as the current lead left the ring. This arrangement adds half of the power dissipated in the leads to the measured power dissipation in the heater.

The sample heater was #40 manganin wire wound non-inductively on the thin copper ring HR (Figure 2). The heater had a nominal resistance of approximately 2000 ohms.

The thermometer was a $\frac{1}{2}$ watt, 10 ohm, carbon composition resistor obtained from Allen-Bradley Company without the insulating case. This resistor was cemented inside of a threaded copper plug with G. E. adhesive. The lower lead wire was grounded to the bottom of the plug. This plug was

then screwed tightly into the well in the top of the can.

The heater circuit is shown in Figure 4. With the main heater switch closed, current from a 4.2 volt Willard low-discharge battery was passed through an attenuator circuit, then through either the calorimeter heater or the exercise resistor, and finally through the 100 ohm standard resistor and a milliammeter. The heater-exercise switch is a SPDT Millisec relay (Stevens-Arnold) which was energized by timing signals from the bench control unit of a Standard Electric Company pendulum clock. The bench control unit could be set for any number of integral seconds up to 2500 seconds with an accuracy of $\pm$ 0.004 seconds. When the relay was not energized the current was routed through the exercise circuit which was adjusted to have the same resistance as the parallel combination of the heater and its shunt. The total current in the circuit was obtained by measuring the emf across the 100 ohm standard resistor. The voltage across the heater was obtained from a measurement of the emf across either the 100 ohm or 100+1000 ohm standard in the heater shunt.

The attenuator was a symmetric T; its application to calorimetry was first proposed by Hoge (44). The properties of this circuit shown in the simplified schematic (Figure 5) are such that X and Y may be so adjusted that the power fed into the load resistance R_L may be varied while the resistance seen by the battery remains constant. Under these conditions a slight change in R_L, such as might occur by virtue of the

Figure 4. Heater circuit.

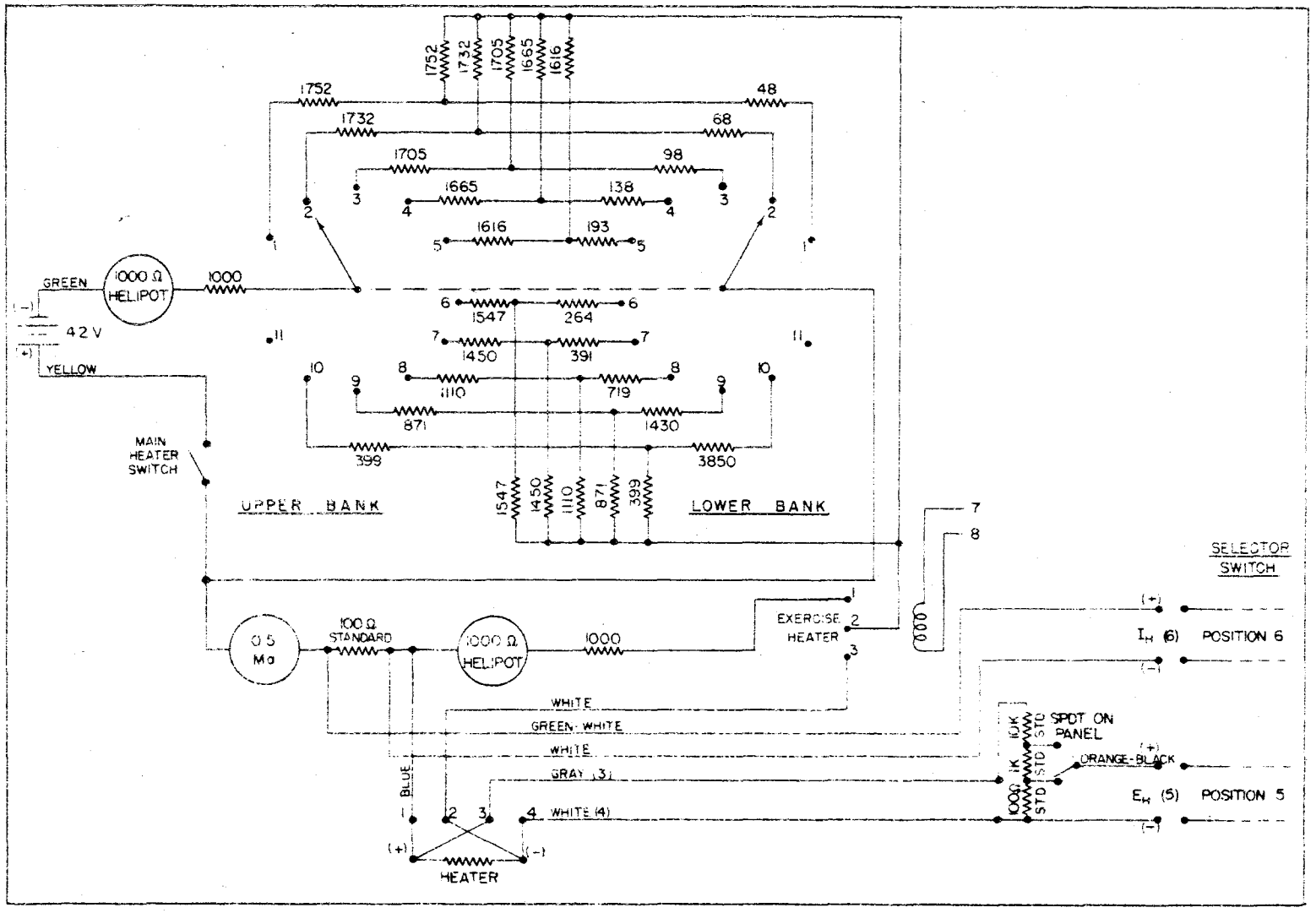
1752
1732
1705
1665
1616
48
68
98
138
193
1547
264
1450
391
1110
719
871
1430
399
3850
GREEN
1000 Ω HELIPOT
1000
42 V
YELLOW
MAIN HEATER SWITCH
UPPER BANK
LOWER BANK
0.5 Ma
100 Ω STANDARD
EXERCISE HEATER
WHITE
GREEN-WHITE
GRAY (3)
BLUE
WHITE (4)
HEATER
SELECTOR SWITCH
I_H (6) POSITION 6
E_H (5) POSITION 5
SPOT ON PANEL
ORANGE-BLACK
10K
1K
STD

Figure 5. Symmetric T attenuator.

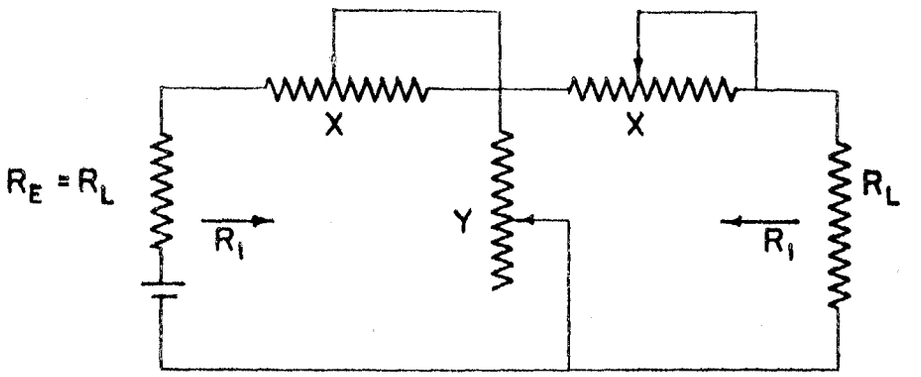
X
X
$R_E = R_L$
R_1
Y
R_1
R_L

temperature coefficient of the heater resistance, does not affect the power dissipation. Under the conditions that the generator and load impedances are made equal to each other and to the image impedance R_1, the values of X and Y may be calculated (45) from the equations

$$X = R_1(\alpha - 1)/(\alpha + 1)$$

$$Y = R_1(2\alpha)/(\alpha^2 - 1)$$

where $\alpha = \frac{\text{heater current without attenuator}}{\text{heater current with attenuator}}$.

The thermometer circuit is shown in Figure 6. With the main thermometer switch closed current from the 2.1 volt Willard low-discharge battery was passed through a milliammeter and then through the combination of parallel resistor and thermometer plus standard resistor. The value of the parallel resistance was chosen so that the power dissipated in the thermometer remained constant at 10^{-8} watts when the thermometer resistance changed from 100 to 3000 ohms.

All emf's were measured on a White double potentiometer. It had a range of 0-99990 microvolts, with one unit on the last dial corresponding to 10 microvolts. A selector switch with silver contacts routed the various emf's to the White from the heater and thermometer circuits. The galvanometer used was a Leeds and Northrup Type 2285, having a sensitivity of approximately 0.0032 μa/mm at one meter. The galvanometer deflection was viewed through a 16 power telescope. The galvanometer mirror reflected a 0-500 mm ground glass scale,

Figure 6. Thermometer circuit.

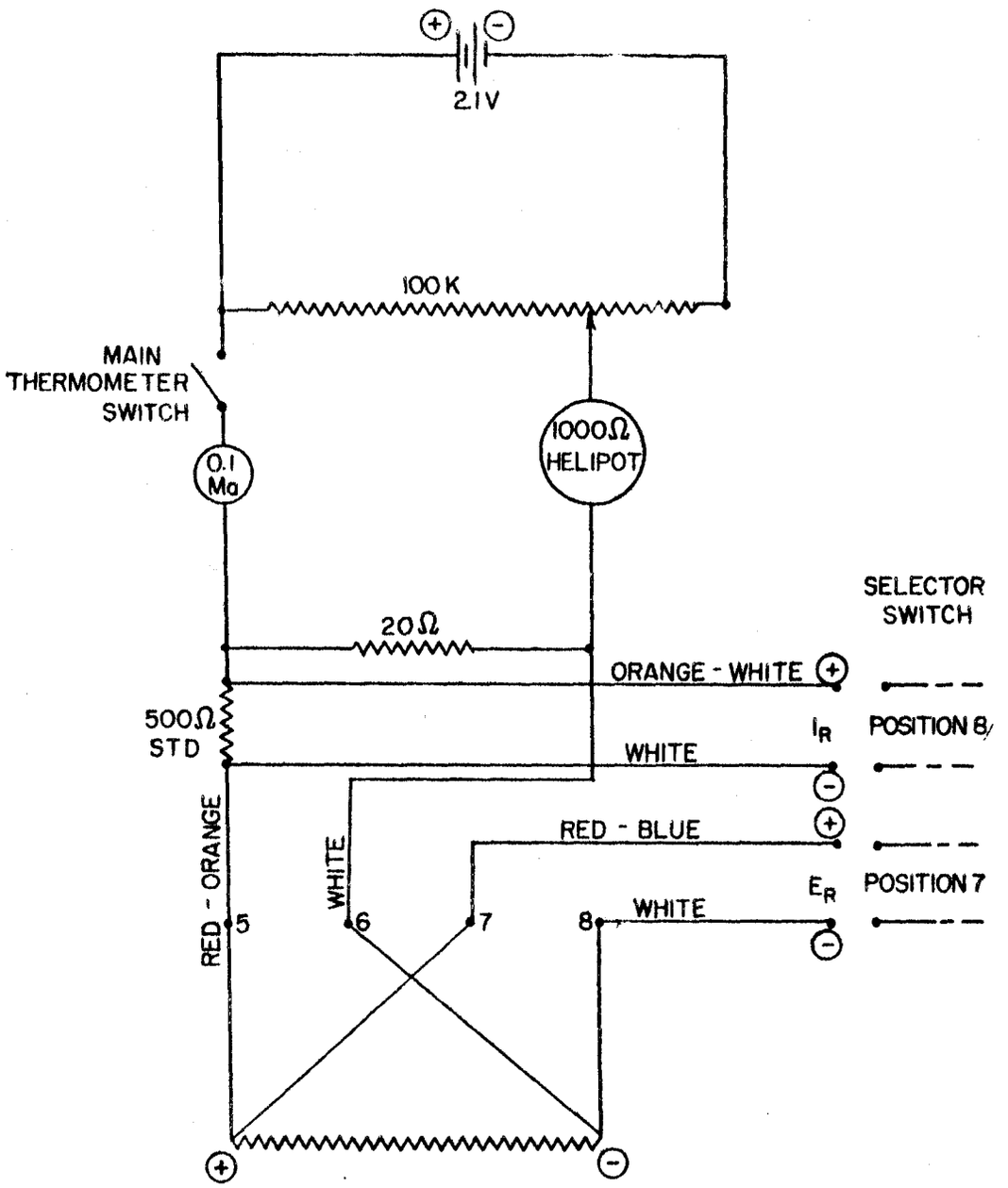
2.1V
100 K
MAIN
THERMOMETER
SWITCH
0.1
Ma
1000Ω
HELIPOT
SELECTOR
SWITCH
20Ω
ORANGE - WHITE
500Ω
STD
I_R
POSITION 8
WHITE
RED - BLUE
RED - ORANGE
WHITE
E_R
POSITION 7
WHITE
5
6
7
8

which was illuminated from behind by a fluorescent light. The scale was approximately 6.5 meters from the galvanometer.

IV. EXPERIMENTAL PROCEDURE

A. General

The liquid helium for use as a refrigerant was prepared in a Collins Helium Cryostat. The liquid was transferred into a 50 liter Superior dewar for storage until needed. Transfer from the storage dewar to the experimental cryostat was accomplished with a vacuum jacketed stainless steel transfer tube. Transfer efficiency was approximately 90 per cent after the initial cooling.

Helium exchange gas was used to cool the sample to the desired temperature. However, problems arose in removing the exchange gas when it was desired to thermally isolate the sample from its surroundings. The degree of adsorption of helium on metal surfaces increases sharply when the temperature is decreased below 4.2°K. Because of this property, some of the helium adsorbed on the sample will desorb during a heating period and tend to re-establish thermal contact with the surroundings. To circumvent this difficulty a technique was developed to cool the sample using the minimum amount of exchange gas.

After the inner dewar had been filled with liquid helium, 1.5×10^{-4} moles of helium gas were admitted to the experimental chamber through the metering volume. This quantity of exchange gas would cool the sample can to 4.2°K. in approximately two hours. The chamber was then opened to its vacuum

system. After approximately five minutes of pumping the fore-pump was isolated from the system and a commercial helium mass spectrometer leak detector used as the backing pump for the system's diffusion pump. Pumping was continued until the leak detector indicated no further helium being removed. The use of a leak detector in such an application was first suggested by Garfunkel and Wexler (46).

The bath temperature was then lowered to approximately 2.6°K. and held constant with the manostat. The calorimeter chamber was next isolated from the pumping system and 7×10^{-5} moles of helium exchange gas admitted. After the sample had reached bath temperature the chamber was again opened to its vacuum system, and pumping continued until the leak detector indicated no further helium being removed. The bath was then pumped to its lowest temperature (1.1°K.), and alternate temperature and power measurements taken from 2.6° to 4.2°K. The bath temperature was then raised to 4.2°K. and the above procedure repeated with 1.6°K. the lowest sample temperature. The quantities of exchange gas used in the various steps were found experimentally to be the minimum quantities consistent with reasonable cooling times.

After all desired heat capacity data had been taken the bath temperature was raised to 4.2°K., 10^{-2} moles of exchange gas added, and the thermometer calibration made. A five watt heater was used to raise the bath temperature.

B. Thermometry

The resistance of the carbon thermometer was calibrated against the vapor pressure of liquid helium in the bulb B (Figure 2). The "agreed" experimental temperature scale (26) of 1955 was used to convert helium vapor pressure to temperature. Temperatures deduced from this scale were denoted by the symbol T_{55E}.

Thermometer calibration points were taken at intervals of 0.2°K. over the temperature region of interest after the heat capacity data had been taken. The resistance thermometer and vapor pressure bulb were thermally coupled by admitting 10^{-2} moles of helium to the calorimeter. An experiment showed this to be adequate coupling: with the bath at its lowest temperature, introduction of an equivalent amount of helium left the thermometer resistance unchanged.

The temperature of the bath was maintained constant to ±0.0005°K. for each calibration point. Temperature control above 2.6°K was attained by regulation of the pressure of helium above the bath with a manostat in the pumping lines. At temperatures below 2.6°K. regulation was attained through use of a Sommers type electronic regulator (47). This regulator used a resistance thermometer in the bath as one arm of a bridge circuit, and a variable resistance as another. The pumping rate was adjusted so that the bath was cooling slowly, and then the variable resistance was set to corre-

spond to the desired bath temperature. The off-balance of the bridge circuit was fed through an amplifier to a heater in the bath. For temperatures above the lambda point of liquid helium, temperatures were always approached from above to avoid the possibility of supercooling the liquid below the surface.

Vapor pressures above 40 mm of mercury were measured with the mercury manometer. Below 40 mm of mercury pressures were measured with the oil manometer. A Wild Cathetometer was used to measure the liquid heights in both manometers. The results from the oil manometer were converted to mm of mercury at the same temperature. To accomplish this conversion, the density of the oil was measured as a function of temperature before introduction into the manometer. This density calibration was checked periodically by comparison with the mercury manometer. The readings on the mercury manometer were corrected for capillary depression using the data of Cawood and Patterson (48). This particular set of data was chosen because the experimental conditions under which it was obtained more closely approximated those of this study. Corrections to standard temperature and gravity were also made.

In order to calibrate the thermometer, an emperical equation was used which defines a resistance temperature T_r. This equation was

(14) $$1/T_r = a^2/\log R + b^2 \log R + 2ab \quad .$$

Two experimental points were used to evaluate the constants a and b. The calibration then consisted of obtaining $T_{55E}-T_r$ as a function of T_r. The constants a and b were found to change considerably after cycling the thermometer between room temperature and 4.2°K. However, if the matching points were chosen at the same temperature, the general shape of the calibration curve remained unchanged.

Thermomolecular pressure drops in the tube connecting the vapor pressure bulb and the manometer system were calculated. At 1.6°K. a 0.03 per cent error in temperature was introduced due to thermomolecular pressure differences. At higher temperatures this error became vanishingly small. In view of this result, the vapor pressure of helium in the bulb was used as the temperature standard at all temperatures. The correction of the temperature of the thermometer due to the hydrostatic head difference between the vapor pressure bulb and the carbon resistance thermometer was not made. This correction was calculated to be negligible at all temperatures with the possible exception of those just above the lambda point. However, there was no evidence for this correction from a discontinuity of the calibration curve at the lambda point.

As previously mentioned, the temperature and power measurements were taken alternately during a run. The quantities necessary for temperature were E_r, the voltage drop across the thermometer, and I_r, the voltage drop across the

standard resistor in series with the thermometer. The quantities E_r and I_r were measured alternately before and after a heating period at time intervals of 30 seconds. Since E_r and I_r were not constant, it was necessary to interpolate each to the time when the other was taken. The resistance R of the thermometer was calculated from the relation

(15) $\quad R = (E_r/I_r)494.80$ ohms

since the resistance of the standard was 494.80 ohms.

Calculation of the initial and final thermometer resistances for a heating period were made by plotting thermometer resistance as a function of time both before and after a heating period. In general, linear drifts were observed. Both plots were extrapolated linearly to the time corresponding to the middle of the heating period. The resulting values of resistance were taken to be R^i and R^f, and converted to resistance temperatures T_r^i and T_r^f. Finally the resistance temperatures were converted to temperatures T_{55E}^i and T_{55E}^f on the "agreed" scale.

C. Heat Input

The proper combination of attenuator setting and time of heating were chosen to give a sample temperature rise of 0.1-0.2°K. during each heating period. The time of the heating period was usually chosen to be 3, 4, or 5 minutes. The energy in joules added to the sample during a heating period was given by

(16) $Q = (I/R_1 - E/R_2)\,(ER_3/R_2)\,t$,

where, I = the emf in volts across R_1

E = the emf in volts across a fraction of the parallel shunt

R_1 = the resistance of the 100 ohm standard series resistor

R_2 = the total resistance of the shunt (including its leads) in parallel with the heater

R_3 = the resistance of that part of the shunt across which E exists

t = the time in seconds that current was flowing through the heater.

Both E and I were observed to remain constant to $\pm$ 0.2 microvolt during a heating period. This was due partly to the circuit design and partly to the small resistance change of the manganin heater over the temperature interval of a heating period.

D. Treatment of Data

The mean gross heat capacity, C_g, was evaluated by the relationship

(17) $C_g = Q/(T^f_{55E} - T^i_{55E})$ joules/deg .

This was taken to be the heat capacity of the sample plus addenda at the average temperature $(T^i_{55E} + T^f_{55E})/2$. The heat capacity of the addenda, C_a, was measured independently and a smooth curve plotted as a function of temperature. The heat

capacity of the sample was then calculated from the relation:

(18) $C = (C_g - C_a)/n$ joules/(mole-deg)

where C = the mean heat capacity of the sample over the temperature range of C_g

C_a = the heat capacity of the addenda at the mean temperature of C_g

n = number of moles of sample.

The use of the above relation assumes that C varies linearly with temperature over the range of the heating period. The corrections for the actual curvature were calculated to be less than 10^{-7} per cent, and were neglected.

At temperatures below 4°K. the heat capacity of simple metals can be represented by the relation

(1) $C = \gamma T + \beta T^3$.

As previously discussed, the coefficients γ and β are related to the electronic and lattice contributions respectively. For the purpose of evaluating the two constants, the heat capacity equation was rewritten as

$$C/T = \gamma + \beta T^2 ,$$

and the data tabulated for C/T as a function of T^2. This then reduced the equation to a linear one of the form $y = \gamma + \beta x$. The best values of the two constants were found by the method of least squares. This required solution of the determinant

$$\begin{vmatrix} x & y & 1 \\ \sum_{i=1}^{n} x_i & \sum_{i=1}^{n} y_i & \sum_{i=1}^{n} 1 \\ \sum_{i=1}^{n} x_i^2 & \sum_{i=1}^{n} x_i y_i & \sum_{i=1}^{n} x_i \end{vmatrix} = 0 \quad ,$$

where n was the number of x-y pairs.

The probable errors, P_γ and P_β, in the values of γ and β obtained from the above determinant were calculated from the relationships

$$P_\gamma = r_e \sqrt{\sum x_i^2 / D} \quad ; \qquad P_\beta = r_e \sqrt{n/D}$$

where $r_e = 0.6745 \sqrt{\sum d_i^2 / (n-2)}$

$D = n \sum x_i^2 - (\sum x_i)^2$

$d_i = y_i - y_i\,(\text{calc})$.

P_γ was the probable error in the electronic heat capacity. The Debye characteristic temperature was derived from the coefficient β by use of the following relation

$$\theta_D = (12 \pi^4 Rn/5\beta)^{1/3} \quad .$$

In this equation n was the number of atoms per formula weight, and the other symbols had their usual meanings. The relative error, $\delta\theta_D$, in the Debye temperature was calculated from the relation

$$\delta\theta_D = \frac{1}{3} \left(\frac{P_\beta}{\beta} + \frac{\delta n}{n} \right) \quad ,$$

where δn was the relative error in n.

V. RESULTS

Calibration data for the resistance thermometer with the addenda and with the addenda plus bronzes having x equal to 0.56, 0.65, 0.73, 0.81 and 0.89 are given in Table 1 - 6 respectively. A typical calibration curve is shown in Figure 7. Uncertainties in temperatures due to uncertainties in the various measurements comprising a temperature determination are shown as vertical lines in Figure 7. The values of the parameters a and b in equation (14) for the various runs are listed in Table 7 in the order in which the runs were made.

Data obtained from the heat capacity measurements on the addenda are tabulated in Table 8. Since the measurements on the addenda and the samples were not made at the same temperatures, it was necessary to smooth the addenda data to combine with the data on the samples. The heat capacity of the addenda has been plotted in Figure 8. The values of C_a taken from this curve were used in equation (13) to calculate the heat capacities of the samples.

Data obtained from the heat capacity measurements on the addenda plus bronzes having x equal to 0.56, 0.65, 0.73, 0.81 and 0.89 are given in Tables 9 - 13 respectively. The columns are average temperature, T_{55E}; change in temperature due to heating, $T^f_{55E} - T^i_{55E} = \Delta T$; the gross heat capacity, $Q/\Delta T = C_g$; and the heat capacity of the sample,

Table 1. Calibration of thermometer with addenda.

R (ohms)	T_R (°K.)	P (mm. of Hg)	T_{55E} (°K.)	$T_{55E}-T_R$ (°K.)
113.05	4.187	743.89	4.188	.001
120.82	4.029	636.51	4.028	-.001
129.62	3.873	543.19	3.873	.000
145.07	3.644	421.62	3.642	-.002
164.12	3.421	322.92	3.417	-.004
191.02	3.178	234.80	3.174	-.004
226.06	2.942	167.49	2.941	-.001
273.01	2.715	115.54	2.714	-.001
367.69	2.415	64.65	2.408	-.007
432.00	2.277	46.80	2.261	-.016
622.14	2.013	22.52	1.981	-.032
1118.0	1.692	6.997	1.650	-.042

Table 2. Calibration of thermometer with $Na_{0.56}WO_3$ sample.

R (ohms)	T_R (°K.)	P (mm. of Hg)	T_{55E} (°K.)	$T_{55E}-T_R$ (°K.)
112.36	4.200	750.06	4.197	-.003
121.82	4.006	622.81	4.006	.000
134.58	3.788	496.10	3.788	.000
158.29	3.475	347.27	3.477	.002
183.58	3.228	253.22	3.229	.001
222.49	2.951	169.24	2.948	-.003
275.02	2.693	111.32	2.693	.000
320.12	2.532	81.64	2.524	-.008
490.27	2.163	35.08	2.141	-.022
909.12	1.779	10.34	1.749	-.030

Table 3. Calibration of thermometer with $Na_{0.65}WO_3$ sample.

R (ohms)	T_R (°K.)	P (mm. of Hg)	T_{55E} (°K.)	$T_{55E}-T_R$ (°K.)
112.17	4.194	747.32	4.193	-.001
126.10	3.930	576.48	3.930	.000
137.54	3.746	474.09	3.746	.000
161.05	3.449	336.06	3.450	.001
189.20	3.186	238.54	3.185	-.001
223.11	2.953	170.69	2.954	.001
267.39	2.731	118.95	2.731	.000
317.12	2.548	84.52	2.542	-.006
379.93	2.376	58.62	2.362	-.014
928.64	1.774	9.981	1.739	-.035
1159.61	1.667	6.426	1.629	-.038

Table 4. Calibration of thermometer with $Na_{0.73}WO_3$ sample.

R (ohms)	T_R (°K.)	P (mm. of Hg)	T_{55E} (°K.)	$T_{55E}-T_R$ (°K.)
112.23	4.202	746.55	4.192	-.010
120.47	4.029	634.04	4.024	-.005
134.96	3.777	490.29	3.777	.000
150.33	3.563	385.94	3.565	.002
175.16	3.295	277.57	3.299	.004
199.92	3.091	211.25	3.098	.007
238.63	2.856	148.02	2.863	.007
274.22	2.686	111.35	2.693	.007
329.20	2.494	77.35	2.497	.003
416.78	2.280	48.62	2.278	-.002
538.25	2.084	29.20	2.072	-.012
705.73	1.908	16.954	1.890	-.018
938.22	1.751	9.662	1.731	-.020

Table 5. Calibration of thermometer with $Na_{0.81}WO_3$ sample.

R (ohms)	T_R (Deg. K.)	P (mm. of Hg)	T_{55E} (Deg. K.)	$T_{55E}-T_R$ (Deg. K.)
113.62	4.206	755.08	4.204	-.002
123.41	4.007	622.88	4.006	-.001
135.61	3.800	502.55	3.800	.000
150.22	3.596	399.38	3.594	-.002
166.57	3.409	319.10	3.408	-.001
189.08	3.203	244.90	3.204	.001
221.08	2.978	176.81	2.977	-.001
254.54	2.799	132.86	2.796	-.003
300.33	2.612	96.27	2.612	.000
364.33	2.421	65.47	2.414	-.007
459.63	2.223	41.23	2.207	-.016
575.23	2.059	26.35	2.035	-.024
777.09	1.872	14.41	1.842	-.030
1110.16	1.687	7.069	1.652	-.035
1695.88	1.508	3.041	1.476	-.041

Table 6. Calibration of thermometer with $Na_{0.89}WO_3$ sample.

R (ohms)	T_R (°K.)	P (mm. of Hg)	T_{55E} (°K.)	$T_{55E}-T_R$ (°K.)
112.15	4.202	754.76	4.203	.001
121.28	4.013	628.11	4.013	.000
136.20	3.760	480.18	3.758	-.002
152.93	3.535	374.84	3.540	.005
178.60	3.269	268.26	3.273	.004
202.30	3.080	207.45	3.085	.005
236.51	2.871	151.04	2.876	.005
271.33	2.707	114.07	2.707	.000
316.32	2.543	84.88	2.545	.002
370.02	2.394	61.52	2.385	-.009
478.04	2.181	36.84	2.161	-.020
568.54	2.057	26.29	2.034	-.023
956.76	1.752	9.33	1.722	-.030

Figure 7. Thermometer calibration in addenda.

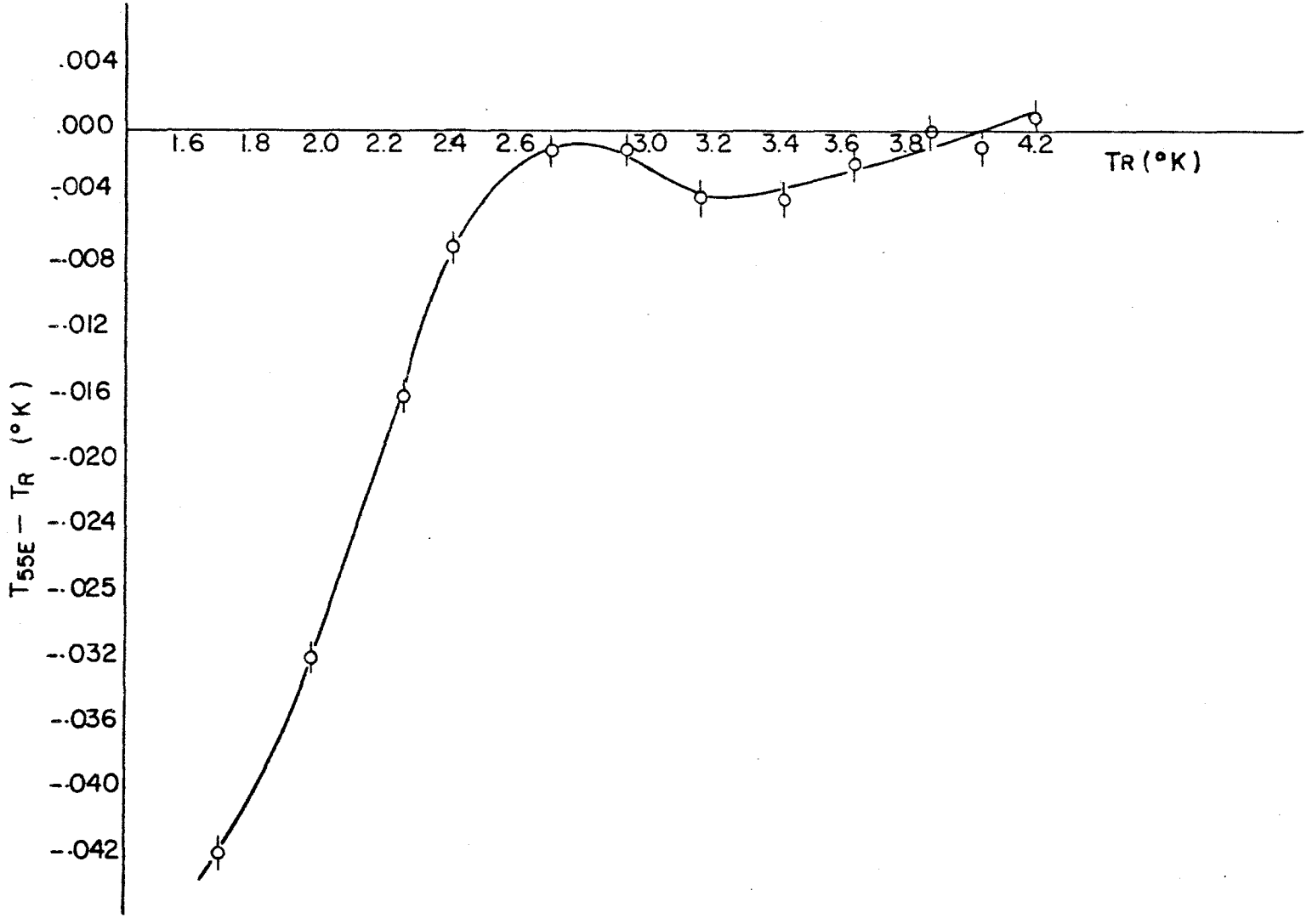
.004
.000
-.004
-.008
-.012
-.016
-.020
-.024
-.025
-.032
-.036
-.040
-.042
1.6
1.8
2.0
2.2
2.4
2.6
3.0
3.2
3.4
3.6
3.8
4.2
TR (°K)
T55E − TR (°K)

Table 7. Calibration equation constants.

Run	a	b
$Na_{0.81}WO_3$	-0.63935	0.65115
Addenda	-0.62427	0.64508
$Na_{0.65}WO_3$	-0.63081	0.64831
$Na_{0.56}WO_3$	-0.63608	0.65092
$Na_{0.89}WO_3$	-0.63578	0.65091
$Na_{0.73}WO_3$	-0.64505	0.65535

Table 8. Experimental values of C_a for addenda, joules-deg^{-1} x 10^2.

T_{55E}	ΔT	C_a
4.213	0.186	1.813
4.021	0.207	1.630
3.824	0.182	1.482
3.625	0.202	1.336
3.439	0.142	1.212
3.272	0.154	1.118
3.106	0.133	1.035
2.932	0.147	0.937
2.805	0.198	0.869
2.743	0.204	0.845
2.674	0.212	0.813
2.568	0.231	0.746
2.441	0.201	0.686
2.309	0.152	0.629
2.173	0.139	0.573
1.985	0.150	0.510
1.794	0.169	0.453
1.595	0.194	0.394

Figure 8. Heat capacity of addenda.

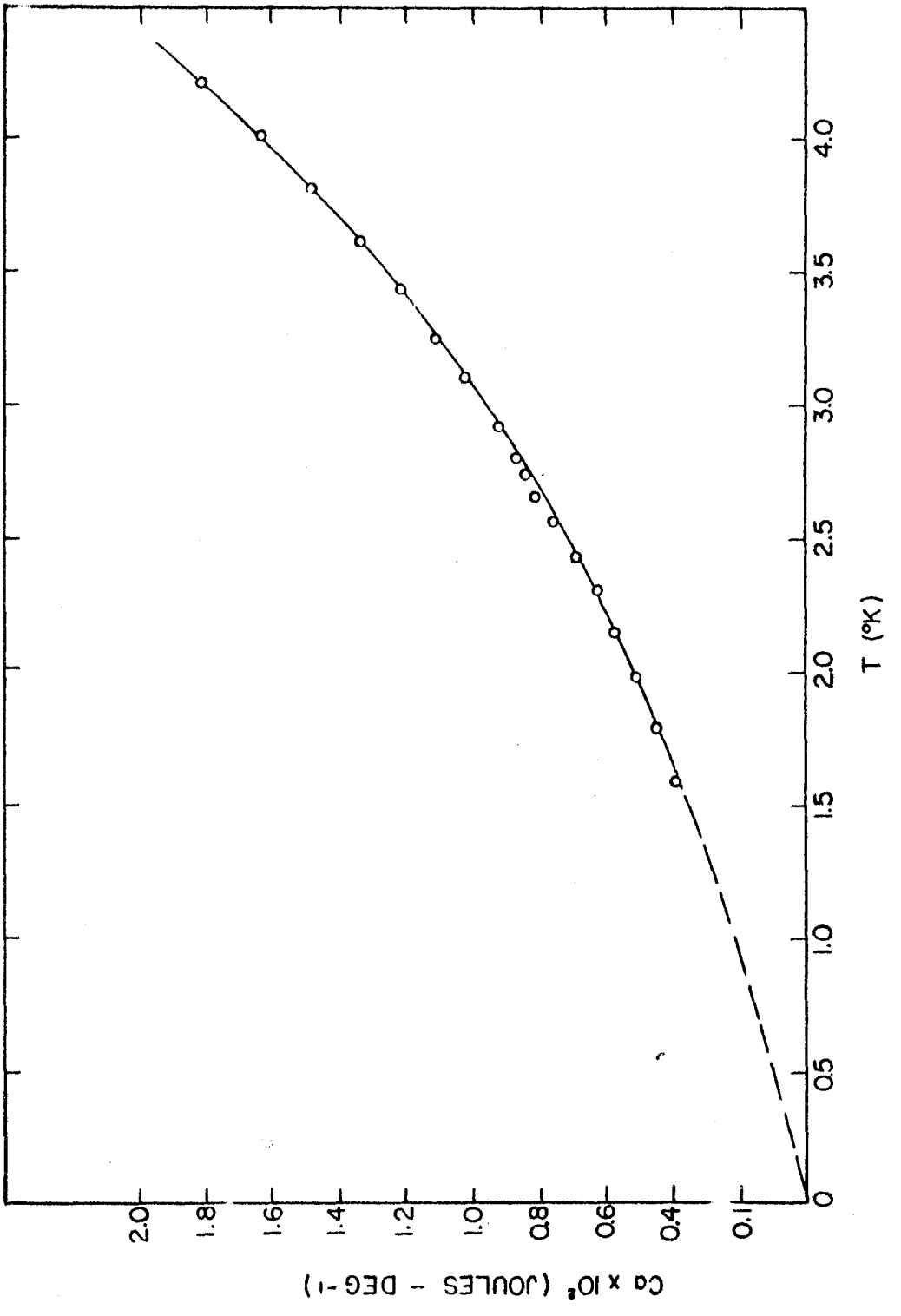
Ca x 10⁶ (JOULES - DEG⁻¹)
2.0
1.8
1.6
1.4
1.2
1.0
0.8
0.6
0.4
0.1
0
0.5
1.0
1.5
2.0
2.5
3.0
3.5
4.0
T (°K)

Table 9. Experimental values of C for $Na_{0.56}WO_3$, joules-deg^{-1}-$mole^{-1}$ x 10^2, n = 0.8563 moles.

T_{55E}	ΔT	C_ε	C
4.059	0.208	2.812	1.342
3.867	0.223	2.565	1.236
3.700	0.141	2.383	1.167
3.565	0.152	2.210	1.066
3.430	0.132	2.036	0.959
3.295	0.140	1.919	0.913
3.137	0.152	1.768	0.841
2.957	0.168	1.599	0.757
2.814	0.181	1.486	0.712
2.741	0.189	1.423	0.685
2.651	0.201	1.338	0.643
2.537	0.220	1.223	0.576
2.420	0.148	1.159	0.564
2.323	0.157	1.093	0.536
2.208	0.135	1.017	0.503
2.078	0.149	0.921	0.446
1.917	0.163	0.842	0.413

Table 10. Experimental values of C for $Na_{0.65}WO_3$, joules-deg^{-1}-$mole^{-1}$ x 10^2, n = 0.8395 moles.

T_{55E}	ΔT	C_g	C
4.140	0.194	3.016	1.516
3.952	0.216	2.709	1.357
3.739	0.237	2.469	1.260
3.549	0.151	2.228	1.121
3.386	0.164	2.051	1.026
3.225	0.141	1.908	0.949
3.067	0.154	1.747	0.878
2.887	0.172	1.564	0.774
2.797	0.179	1.505	0.760
2.706	0.189	1.425	0.724
2.588	0.205	1.314	0.665
2.459	0.139	1.236	0.647
2.341	0.153	1.123	0.573
2.192	0.140	1.022	0.527
2.016	0.150	0.916	0.473
1.794	0.176	0.780	0.392

Table 11. Experimental values of C for $Na_{0.73}WO_3$, joules-deg^{-1}-$mole^{-1}$ x 10^2, n = 0.8183 moles.

T_{55E}	ΔT	C_g	C
4.090	0.208	2.801	1.354
3.903	0.228	2.556	1.250
3.739	0.143	2.352	1.150
3.609	0.151	2.233	1.111
3.466	0.162	2.076	1.025
3.326	0.139	1.940	0.945
3.191	0.149	1.808	0.891
3.042	0.162	1.660	0.811
2.875	0.176	1.529	0.759
2.719	0.189	1.424	0.733
2.642	0.201	1.339	0.679
2.540	0.213	1.264	0.651
2.437	0.142	1.203	0.635
2.353	0.154	1.114	0.571
2.254	0.130	1.052	0.546
2.143	0.141	0.975	0.505
1.991	0.155	0.887	0.459
1.848	0.167	0.819	0.430

Table 12. Experimental values of C for $Na_{0.81}WO_3$, joules-deg^{-1}-$mole^{-1}$ x 10^2, n = 1.002 moles.

T_{55E} (°K.)	ΔT	C_g	C
4.149	0.161	3.505	1.749
3.968	0.175	3.225	1.639
3.763	0.195	2.894	1.462
3.525	0.212	2.662	1.386
3.302	0.134	2.393	1.249
3.126	0.120	2.138	1.094
2.935	0.133	1.930	0.988
2.845	0.138	1.852	0.957
2.763	0.145	1.768	0.918
2.666	0.339	1.636	0.838
2.624	0.155	1.657	0.881
2.467	0.0870	1.492	0.793
2.408	0.114	1.423	0.750
2.394	0.225	1.402	0.736
2.279	0.124	1.308	0.692
2.110	0.0814	1.196	0.645
1.953	0.123	1.079	0.579

Table 13. Experimental values of C for $Na_{0.89}WO_3$, joules-deg^{-1}-$mole^{-1}$ x 10^2, n = 0.9135 moles.

T_{55E}	ΔT	C_g	C
4.166	0.178	3.279	1.653
3.987	0.193	3.032	1.569
3.795	0.208	2.825	1.502
3.627	0.128	2.618	1.405
3.494	0.138	2.439	1.297
3.346	0.148	2.277	1.216
3.184	0.159	2.117	1.141
3.009	0.174	1.932	1.043
2.745	0.197	1.710	0.995
2.667	0.164	1.636	0.920
2.590	0.174	1.534	0.867
2.493	0.187	1.436	0.796
2.373	0.200	1.343	0.752
2.240	0.138	1.243	0.705
2.122	0.147	1.163	0.667
1.963	0.161	1.064	0.615
1.869	0.172	0.995	0.571

Table 14. Electronic specific heat and Debye temperature of sodium tungsten bronze.

Sample	$\gamma \times 10^3$ (joules-mole^{-1}-deg^{-2})	θ_D (°K.)
$Na_{0.56}WO_3$	1.760 ± .022	453.5 ± 3.7
$Na_{0.65}WO_3$	1.922 ± .019	449.2 ± 3.0
$Na_{0.73}WO_3$	2.050 ± .019	496.7 ± 4.6
$Na_{0.81}WO_3$	2.557 ± .032	453.7 ± 5.1
$Na_{0.89}WO_3$	2.819 ± .027	505.1 ± 6.3

$(C_g - C_a)/n = C$.

If C/T is written as a function of T^2, equation (1) yields a straight line with intercept γ, and slope β. The data for the five bronzes are plotted in this way in Figures 9 - 13. It is seen that a straight line is a good approximation to the data for all five samples. The constants of the lines and their probable errors were determined by the method of least squares as previously discussed. These derived quantities are given in Table 14.

Errors in a heat capacity determination at a temperature T may arise through uncertainties in measurements of the energy supplied to the sample, the mean value of the temperature, and the temperature rise of the sample.

The energy which was supplied to the sample was determined by measurements of heater current and potential drop,

Figure 9. Heat capacity of $Na_{0.56}WO_3$.

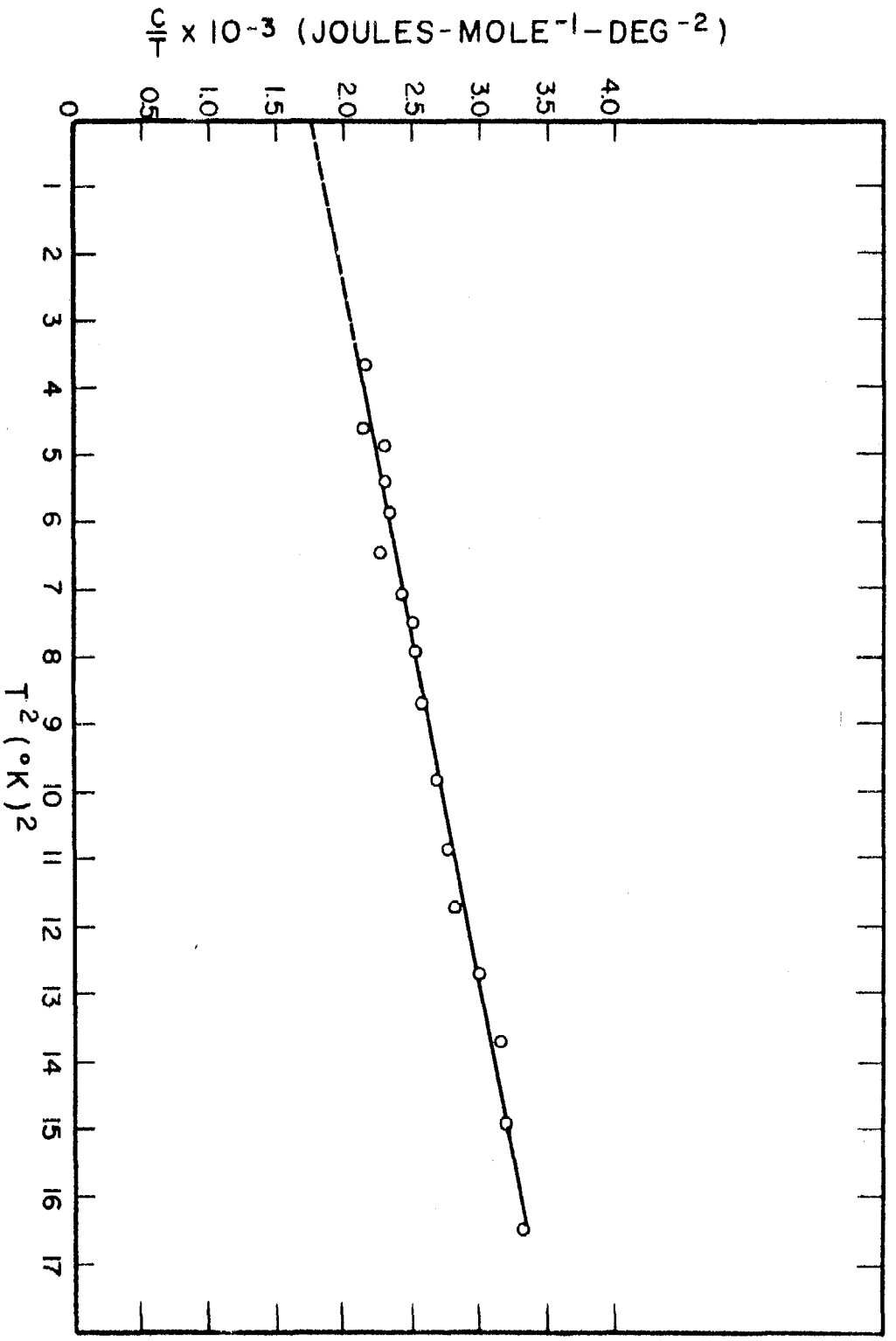
C/T x 10⁻³ (JOULES-MOLE⁻¹-DEG⁻²)
0
0.5
1.0
1.5
2.0
2.5
3.0
3.5
4.0
T² (°K)²
1
2
3
4
5
6
7
8
9
10
11
12
13
14
15
16
17

Figure 10. Heat capacity of $Na_{0.65}WO_3$.

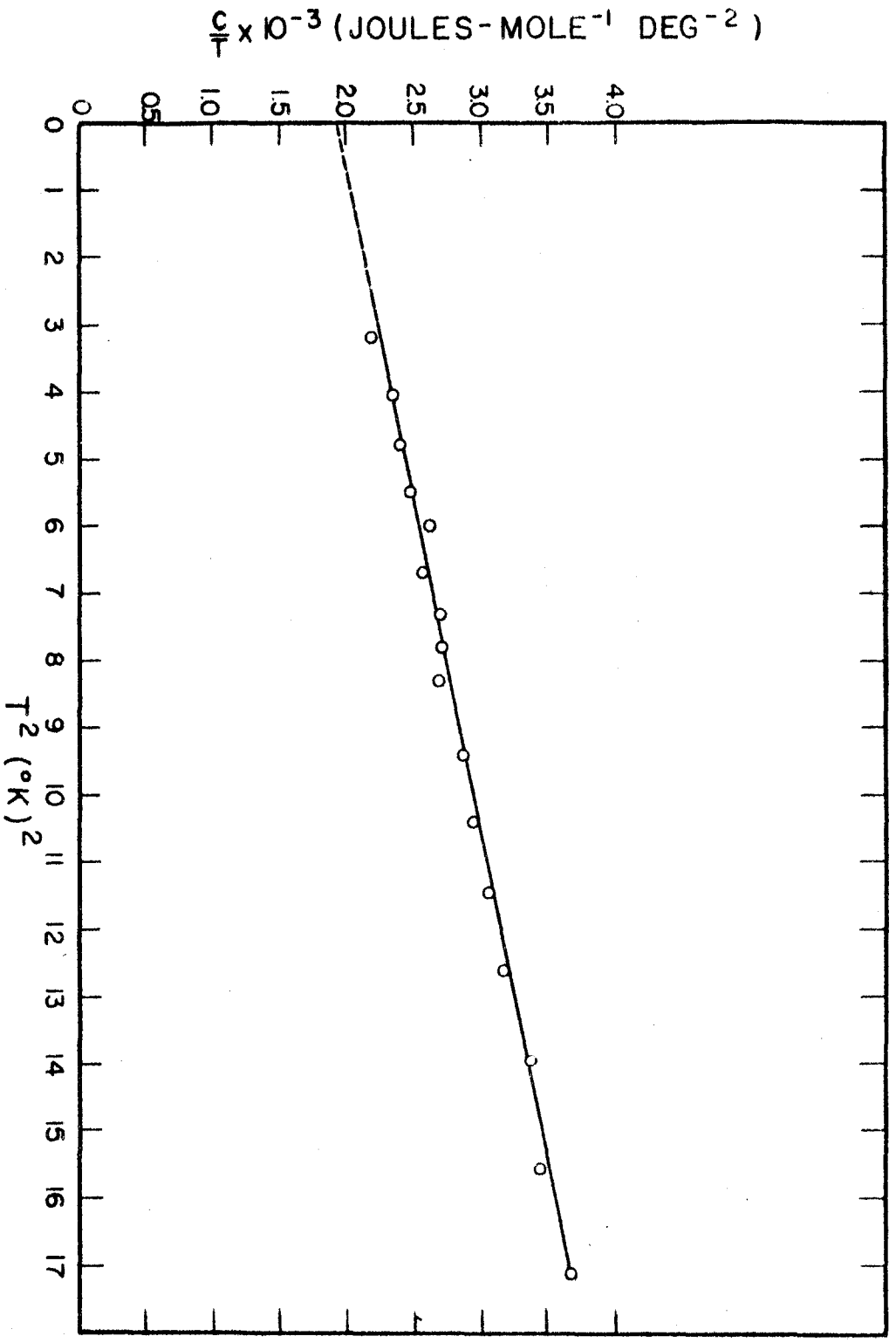
$\frac{C}{T} \times 10^{-3}$ (JOULES-MOLE^{-1} DEG^{-2})
0
0.5
1.0
1.5
2.0
2.5
3.0
3.5
4.0
T^2 (°K)^2
0
1
2
3
4
5
6
7
8
9
10
11
12
13
14
15
16
17

Figure 11. Heat capacity of $Na_{0.73}WO_3$.

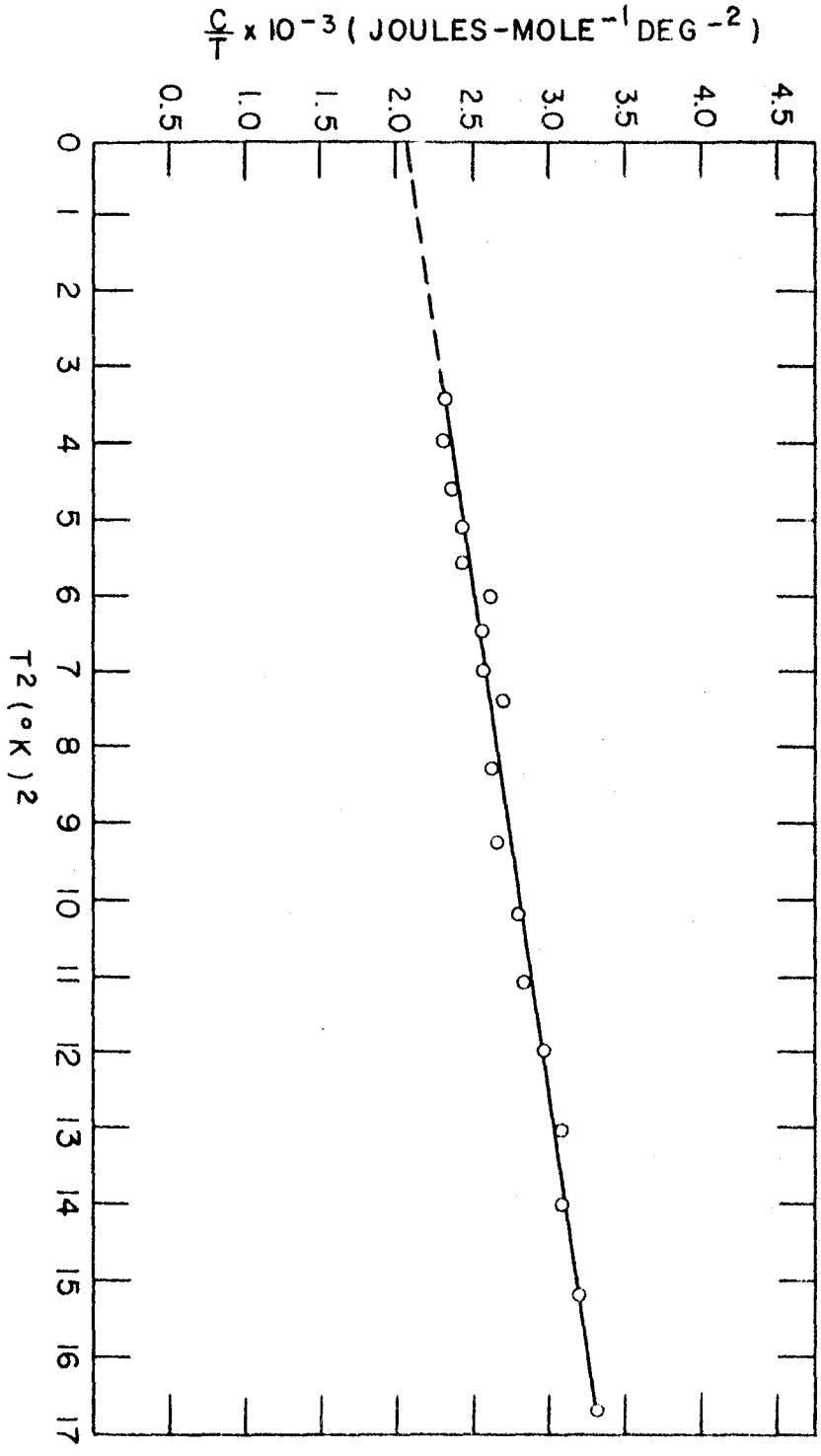
$\frac{C_p}{T} \times 10^{-3}$ (JOULES-MOLE^{-1} DEG^{-2})
0.5
1.0
1.5
2.0
2.5
3.0
3.5
4.0
4.5
0
1
2
3
4
5
6
7
8
9
10
11
12
13
14
15
16
17
T^2 (°K)^2

Figure 12. Heat capacity of $Na_{0.81}WO_3$.

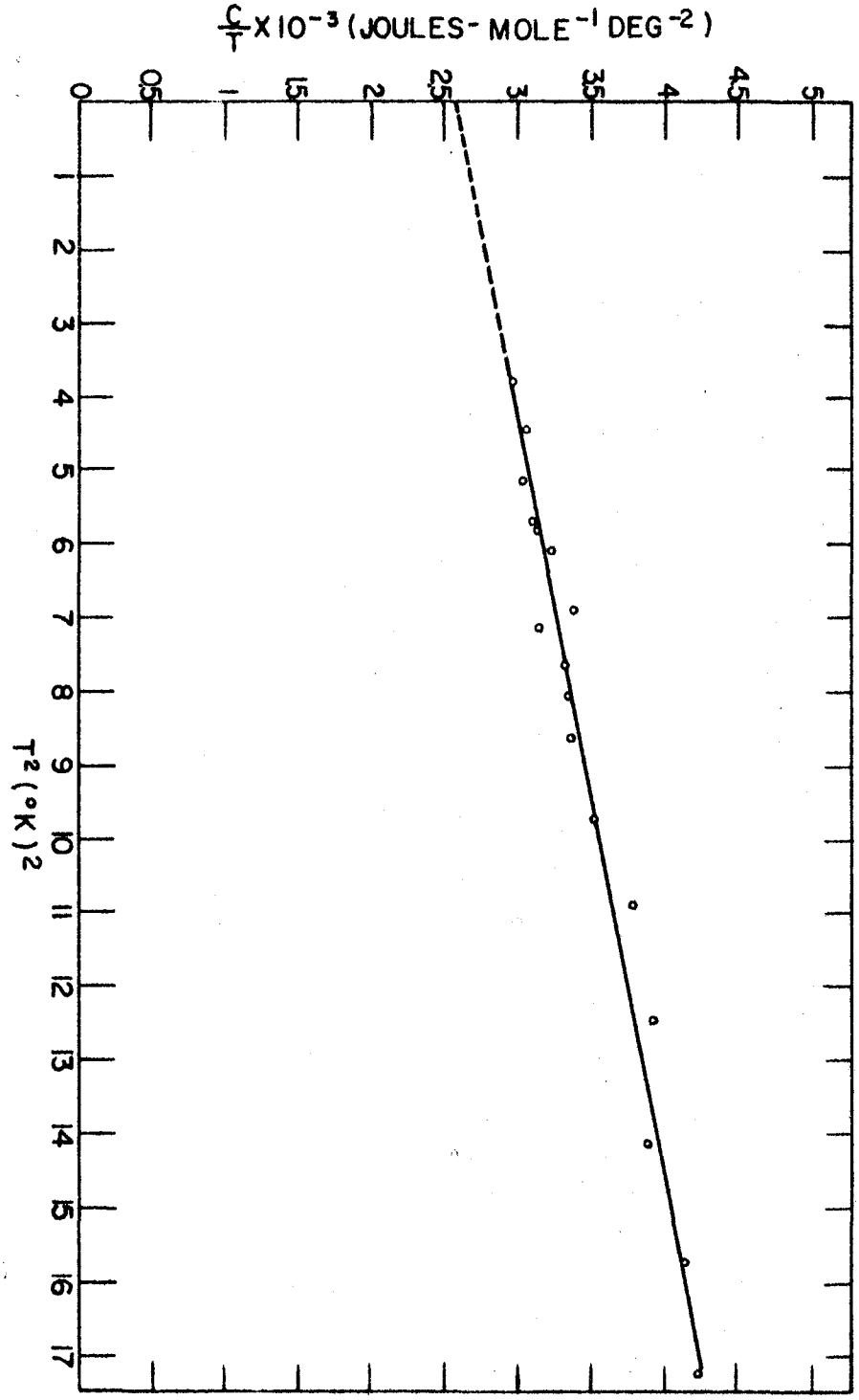
$\frac{C_v}{T} \times 10^{-3}$ (JOULES-MOLE^{-1} DEG^{-2})
0
0.5
1
1.5
2
2.5
3
3.5
4
4.5
5
1
2
3
4
5
6
7
8
9
10
11
12
13
14
15
16
17
T^2 (°K)^2

Figure 13. Heat capacity of $Na_{0.89}WO_3$.

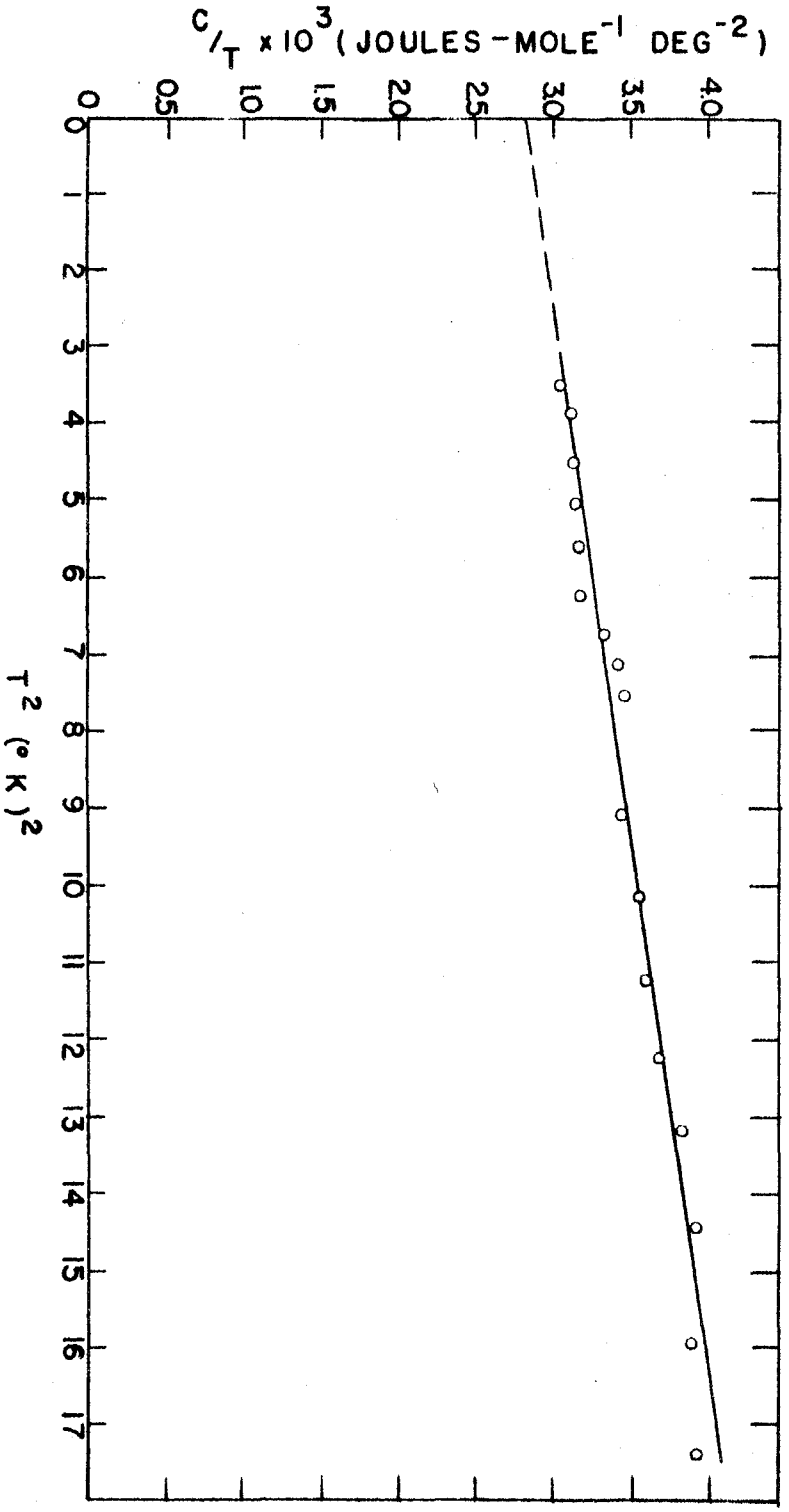
C/T x 10^3 (JOULES-MOLE^-1 DEG^-2)
0
0.5
1.0
1.5
2.0
2.5
3.0
3.5
4.0
T^2 (°K)^2
0
1
2
3
4
5
6
7
8
9
10
11
12
13
14
15
16
17

and time of heating. All of these quantities had uncertainties of less than 0.05 per cent, and were therefore not significant sources of error. The fact that the sample surrounded the heater insured that all of the energy supplied entered the sample.

Errors in the mean temperature of a heating period can arise from uncertainties in the thermometer current and potential drop, and from inaccuracies in the calibration. The uncertainties in the electrical measurements were less than 0.05 per cent. Errors arising from the graphical interpolation of the temperature calibration curves have been estimated to be less than 0.1 per cent except at the lowest temperatures. Errors in heat capacity introduced by the uncertainty of the temperature scale are expected to be everywhere less than 0.5 per cent.

The uncertainty in the temperature rise due to heating introduced the largest source of error in the experiment. This was due mostly to uncertainties in the initial and final resistances obtained from the resistance vs. time plot. At the lowest temperatures, the drift rates were large, thus increasing the uncertainty in the extrapolation. The errors in heat capacity due to this uncertainty in extrapolation have been estimated to be less than one per cent except at the lowest temperatures.

The errors that have been estimated above yield a total uncertainty of 1.5 per cent or less in a heat capacity deter-

mination. Due to the small lattice heat capacity and high molecular weight of the bronzes in addition to the requirement of containing them in a can, the heat capacity of the addenda was comparable to that of the samples. This introduced an additional source of error of less than 1.5 per cent. The total absolute error in the heat capacity of the bronzes was therefore estimated to be less than 3 per cent.

VI. DISCUSSION

To obtain the density of electronic energy levels at the Fermi energy from the electronic specific heat, equation (10b) was rewritten as

(19) $g(\mathcal{E}_F) = 3\gamma n/\pi^2 kRz$.

For the bronzes, z = x and $n = x/a^3$, where a is the lattice parameter. Substituting these quantities and the numerical values of the physical constants into equation (19) gave

(20) $g(\mathcal{E}_F) = 4.242(10^{26})\gamma/a^3$ (energy levels-e.v.$^{-1}$-cm^{-3}).

In this equation γ must be given the units of joules-mole^{-1}-deg^{-2}, and a must be expressed in Angstroms. Hence, the data will yield the density of states at the Fermi level as a function of x; or alternatively, as a function of n since $x = na^3$. A plot of the density of states as a function of energy can be made if it is assumed that the shape of this curve does not vary with sodium concentration.

In order to determine the energy corresponding to a given value of electron density n, equation (4) was differentiated to give

(21) $dn = g(\mathcal{E})\, f(\mathcal{E})\, d\mathcal{E}$.

It was then assumed that $f(\mathcal{E}) = 1$ for all energies less than the Fermi energy and zero for all other energies. This assumption is strictly true only for T = 0°K., but the maximum experimental temperature of 4.2°K. would not be expected to cause significant deviation from this assumption. Rearranging

equation (21), writing the density of states as a function of n, and integrating between limits gave

$$(22) \qquad \int_{\mathcal{E}_1}^{\mathcal{E}_2} d\mathcal{E} = \int_{n_1}^{n_2} dn/g(n) \quad .$$

$\mathcal{E}_1$ and $\mathcal{E}_2$ are energies corresponding to electron densities n_1 and n_2 respectively. Therefore, if $1/g(n)$ is plotted as a function of n, the area under this curve between any two values of n corresponds to their energy difference. This graphical integration is shown in Figure 14. The area increments were chosen small enough so that the trapezoidal rule gave an accuracy in accord with the data.

The density of states as a function of $(\mathcal{E} - \mathcal{E}_o)$ is plotted in Figure 15. $\mathcal{E}_o$ is the energy corresponding to the lowest experimental electron density, and cannot be given a numerical value without making some additional assumptions.

As previously mentioned, the construction of the density of states curve is based on the assumption that this curve is the same for all of the bronzes. In order to test the validity of this assumption, the detailed behavior of the density of states must be studied. If it is assumed that each electron in the crystal can be characterized by a wave propogation vector $\vec{k}$, each point formed by the tip of one of the $\vec{k}$ vectors may be regarded as a possible electronic state for the system. On this model it can be shown (49) that the number of states per unit volume per unit energy is given by

Figure 14. Curve for graphical integration.

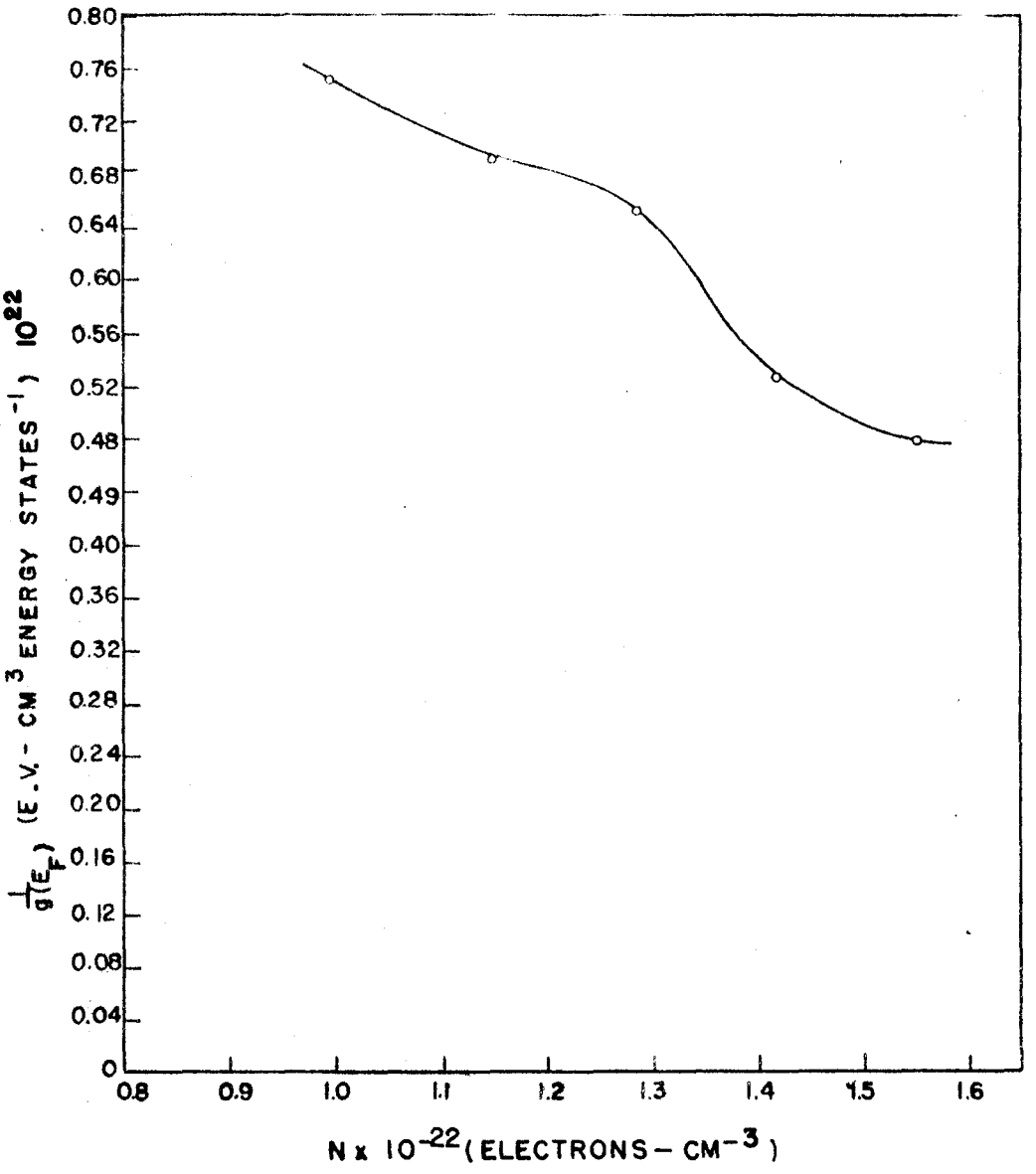
0.80
0.76
0.72
0.68
0.64
0.60
0.56
0.52
0.48
0.49
0.40
0.36
0.32
0.28
0.24
0.20
0.16
0.12
0.08
0.04
0
0.8
0.9
1.0
1.1
1.2
1.3
1.4
1.5
1.6
$\frac{1}{g(E_F)}$ (E.V.- CM^3 ENERGY STATES^{-1}) 10^{22}
N x 10^{-22} (ELECTRONS – CM^{-3})

Figure 15. Density of states curve.

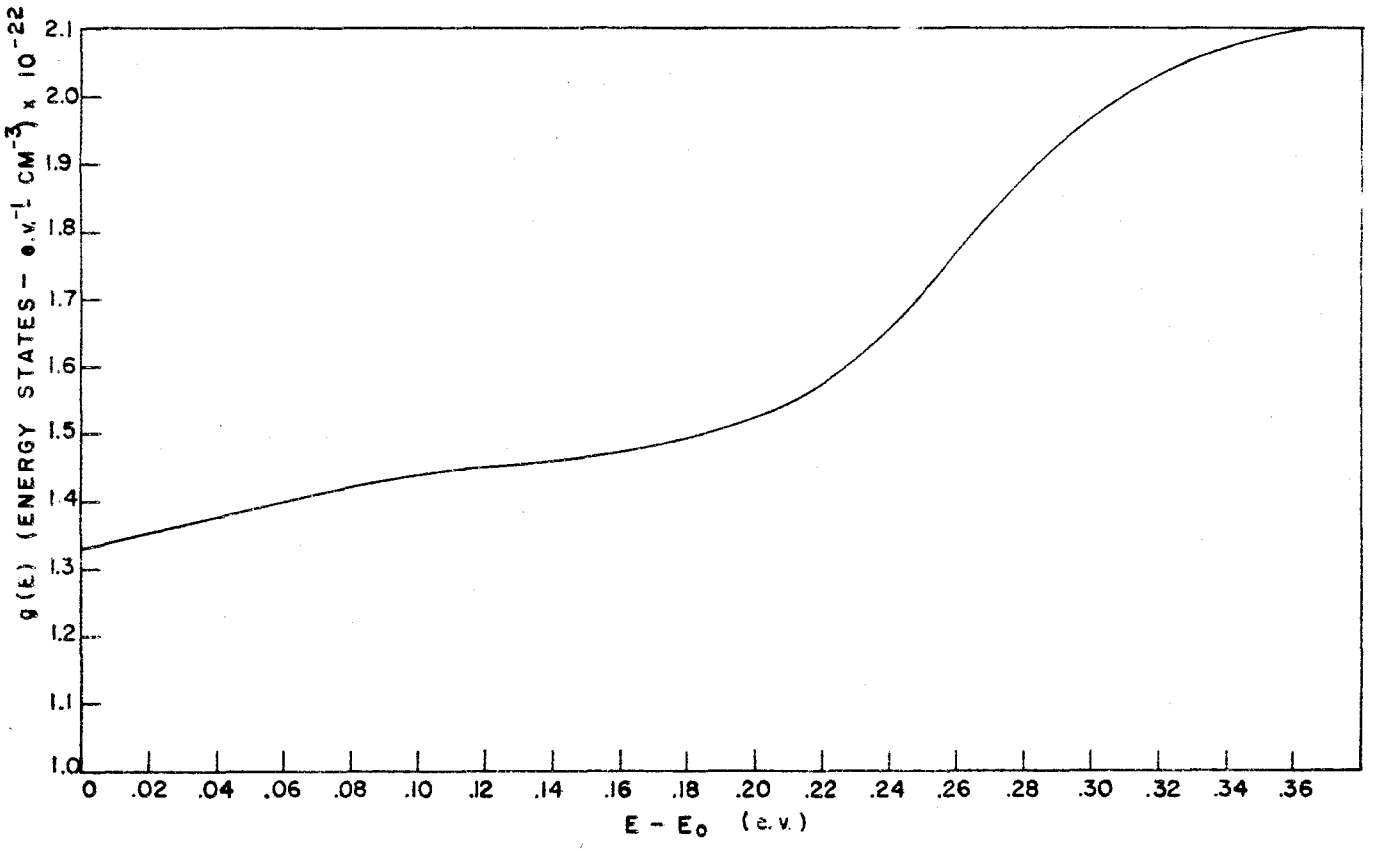
g(E) (ENERGY STATES - e.v.$^{-1}$ CM^{-3}) x 10^{-22}
2.1
2.0
1.9
1.8
1.7
1.6
1.5
1.4
1.3
1.2
1.1
1.0
0
.02
.04
.06
.08
.10
.12
.14
.16
.18
.20
.22
.24
.26
.28
.30
.32
.34
.36
E - E$_0$ (e.v.)

the surface integral

$$(23) \qquad g(\mathcal{E}) = \frac{1}{4\pi^2} \int \frac{dS}{|\text{grad}_k \mathcal{E}(\vec{k})|} \quad ,$$

in which dS is the differential area of the surface of constant energy in $\vec{k}$ space, and $\mathcal{E}(\vec{k})$ is the electronic energy.

In order to determine the effect of a change in sodium concentration on $g(\mathcal{E})$, the perturbations on the constant energy surface and on the electronic energy caused by the addition of sodium must be considered. Such perturbations might arise because varying x in the formula Na_xWO_3 changes not only the electron density, but also changes the potential field in which the electrons move by changing the density of sodium cores.

The lattice periodicity gives rise to the zone structure of a solid, which influences the surface of constant energy and hence the density of states. The zone structure is a function of crystallographic symmetry and interatomic spacing only. The cubic bronzes all have the perovskite structure with tungsten at $(\frac{1}{2}\frac{1}{2}\frac{1}{2})$, oxygen at $(\frac{1}{2}\frac{1}{2}0)$, $(\frac{1}{2}0\frac{1}{2})$ and $(0\frac{1}{2}\frac{1}{2})$, and sodium sites at (000). The sodium sites have a probability of occupancy equal to x, but the crystallographic symmetry remains the same for all x if the sodium distribution is random. There is no experimental evidence to indicate other than a random sodium distribution. Therefore, if the small change in lattice parameter is neglected, the Brillouin zone structure of the cubic bronzes is unchanged by varia-

tions in sodium concentration.

The effect of the sodium core density on the gradient of the electronic energy is more subtle. In order to obtain the energy as a function of k, some simplifying model of a metal must be adopted. By employing the cellular approximation with Bloch one-electron wave functions, the energy is found to be given by

$$(24) \qquad \mathcal{E} = \mathcal{E}_0 + h^2k^2/2m^* \quad .$$

The gradient of this expression can be influenced by the core density only through the effective mass m^*, since all other effects of the lattice are included in the constant $\mathcal{E}_0$ term. This treatment is quite crude, and would be expected to break down badly at values of k near a zone boundary. As discussed previously, attempts to refine this approach have resulted in greater divergence between theory and experiment unless a shielded Coulomb potential is employed (35). The recent work of Bohm and Pines gives some justification for using such a potential on the basis of the collective correlated description of electron motion. Using this approach, Pines (50) calculated the effect of the lattice on the electronic energy and concluded that the terms in the electronic energy equation which are dependent on the lattice tend to cancel one another. To this approximation the construction of the density of states curve for the bronzes is justified. At most, any effect should be small and vary smoothly with

sodium concentration.

The sudden rise in the density of states curve (Figure 15) was not expected, and is quite different from the parabolic shape predicted on the basis of simple free electron theory. One simple model which is consistent with the observed results is based on the filling of a zone in $\vec{k}$ space. The Fermi energy increases with the density of electrons as the sodium concentration of the bronzes is increased. For small values of $\mathcal{E}$ the contours of constant energy in $\vec{k}$ space are spheres, so that $g(\mathcal{E})$ is proportional to $\mathcal{E}^{\frac{1}{2}}$. As $\mathcal{E}$ approaches the energy corresponding to a zone boundary, the contours deviate from spherical shape, and $g(\mathcal{E})$ increases more rapidly than $\mathcal{E}^{\frac{1}{2}}$ until it reaches a maximum when the contour just touches the boundary. On this model, the zone boundary has not yet been reached at the highest experimental point because $g(\mathcal{E})$ is still increasing. The concept of a zone becoming full may account for the difficulty found in preparing bronzes with high sodium concentrations, especially if there is a large energy discontinuity at the zone boundary.

Consideration of the effective electronic mass presents a slightly different way of approaching the problem. The ratio m^*/m can be calculated by taking the ratio of the observed electronic specific heat to the value calculated from the Sommerfeld formula, equation (13). The effective mass as a function of sodium concentration is shown in Figure 16. The rise is quite sharp, and it would be difficult, if not impos-

Figure 16. Variation of effective mass with sodium concentration.

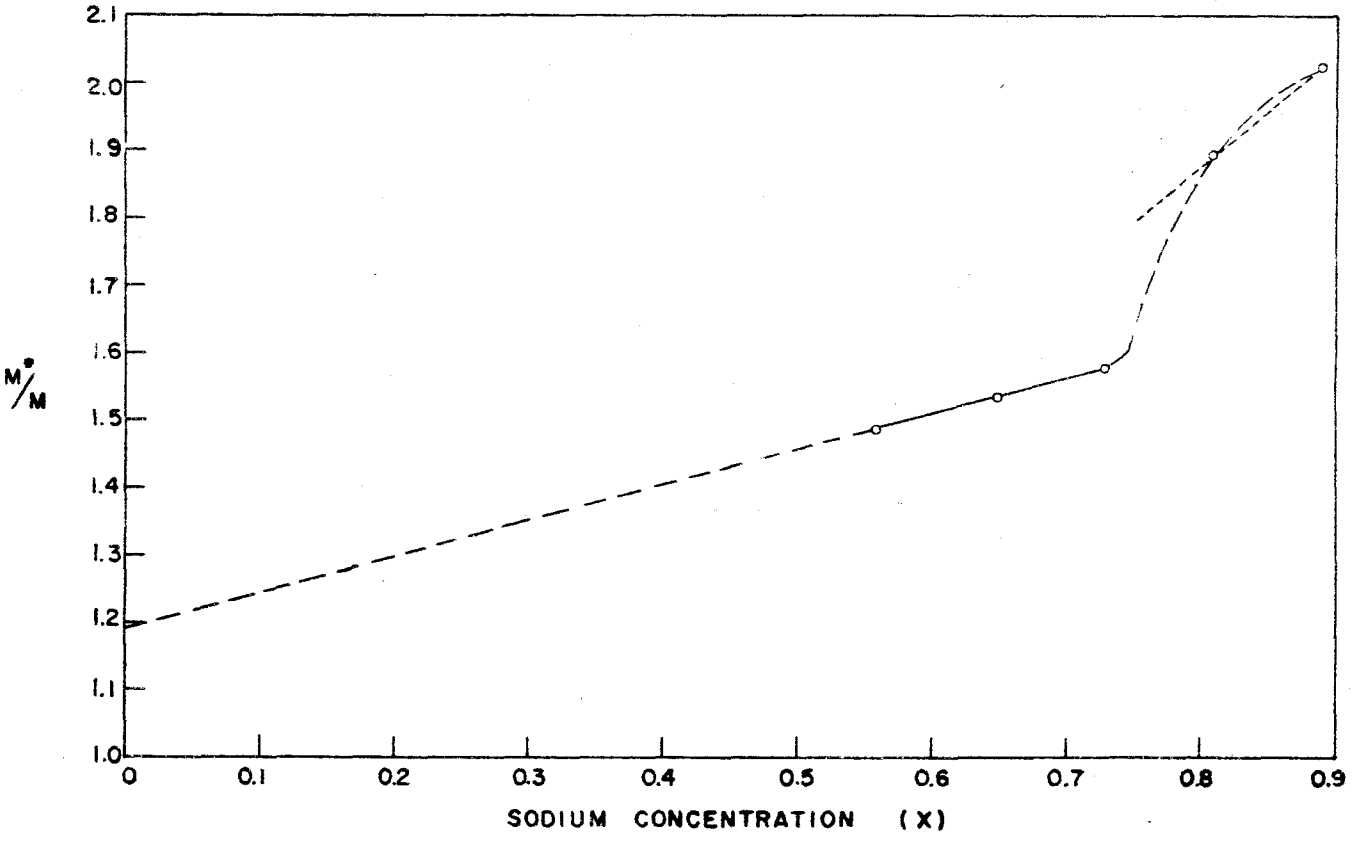
2.1
2.0
1.9
1.8
1.7
1.6
1.5
1.4
1.3
1.2
1.1
1.0
M*/M
0
0.1
0.2
0.3
0.4
0.5
0.6
0.7
0.8
0.9
SODIUM CONCENTRATION (X)

sible, to take enough experimental points to establish whether this is a smooth curve or if there is a discontinuity. An alternate interpretation of the data is presented by the effective mass approximation. To wit, that the density of states for each bronze is parabolic with a curvature defined by the effective mass. However, this conclusion is inconsistent with the fact that the density of states should at most be a simple, slowly varying function of sodium concentration. On the other hand, the change in effective mass is consistent with the idea of a zone becoming full. The effective mass, which is inversely proportional to the curvature of the $\mathcal{E}$ vs. k curve, would be expected to increase rapidly near a zone boundary.

An approximation of the complete density of states curve can be drawn by extrapolating the linear portion of the effective mass vs. sodium concentration curve to x = 0. The equation of the line is

$$(25) \quad m^*/m = 0.535x + 1.190 \quad .$$

Since x is known as a function of electron density n, this equation becomes

$$(26) \quad m^*/m = 3.125(10^{-23})n + 1.180 \quad .$$

Under the assumption that equation (26) is valid, the density of states is given by the free electron result using this value for electronic mass,

$$(27) \qquad g(n) = \frac{4\pi(2m^*)}{h^2}(3n/8\pi)^{1/3} = A(m^*/m)n^{1/3} \quad .$$

In this equation A includes all of the physical constants and is equal to $4.115(10^{14})$ e.v.$^{-1}$-cm^{-2}. Therefore, the energy in electron volts corresponding to any n in the linear portion of Figure 16 is

$$(28) \qquad \mathcal{E} = \int_0^n \frac{dn}{g(n)} = \frac{1}{A}\int_0^n \frac{dn}{(m^*/m)n^{1/3}}$$

$$\mathcal{E} = \frac{1}{A}\int_0^n \frac{dn}{[3.125(10^{-23})n + 1.180]\, n^{1/3}} \quad .$$

This integral can be converted to a tabulated form by making the substitution $u^3 = n$. This reduces equation (28) to the form

$$(29) \qquad \mathcal{E} = \frac{3}{A}\int_0^{n^{1/3}} \frac{udu}{a + bu^3} \quad ,$$

with a = 1.180 and b = $3.125(10^{-23})$.

With n = $0.996(10^{22})$, the value for x = 0.56, equation (29) gives an energy of 1.299 electron volts. This is the value of $\mathcal{E}_o$ in Figure 15 on the basis of this approximation. By calculating the density of states from equation (27) and the corresponding energy from equation (29) for energies below 1.299 electron volts, a complete density of states curve can be drawn. This curve is shown in Figure 17.

The interpretation of the density of states curve in

Figure 17. Complete density of states curve.

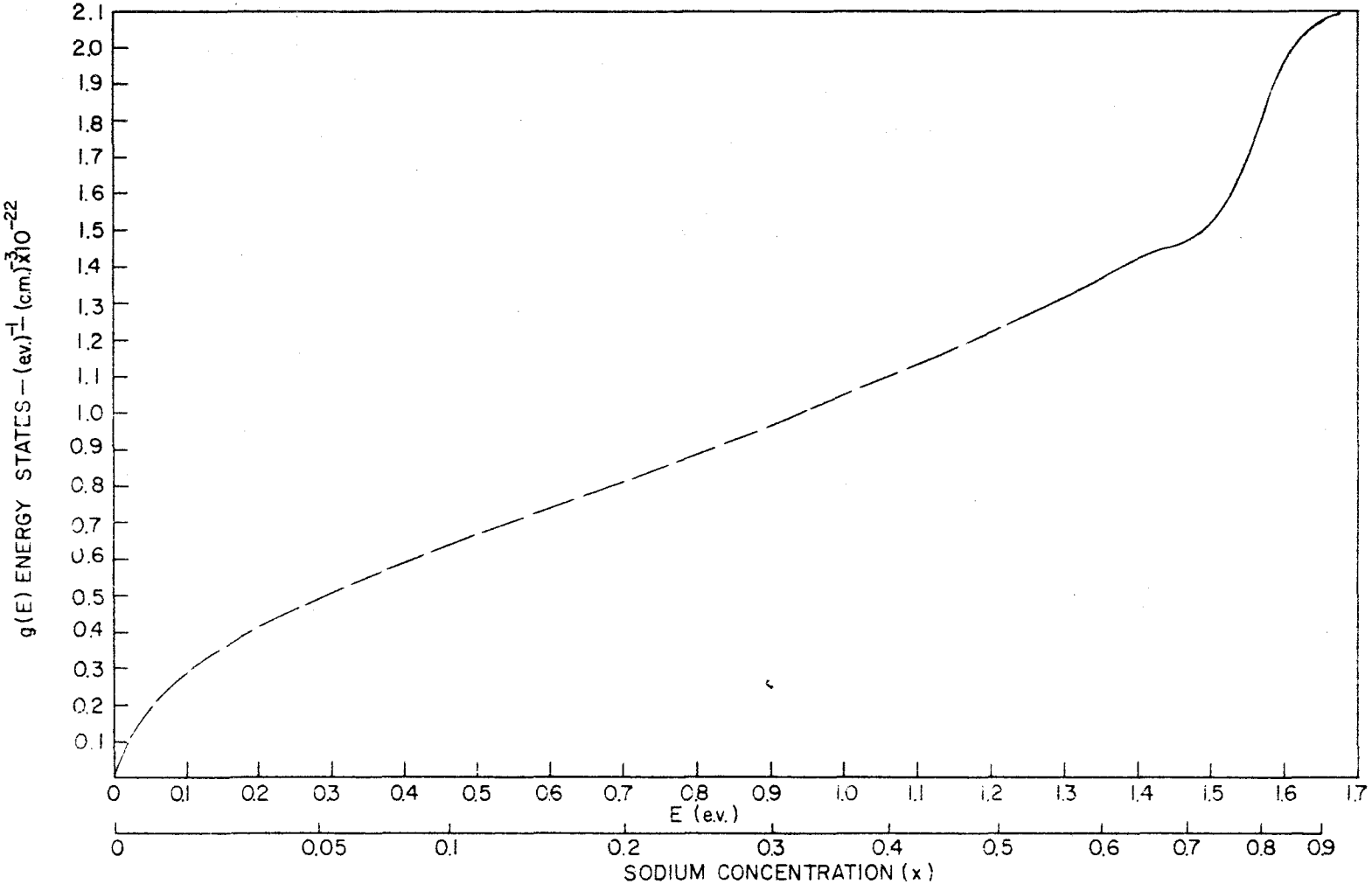
g(E) ENERGY STATES – (ev.)$^{-1}$ – (c.m.)$^{-3}$ X10^{-22}
2.1
2.0
1.9
1.8
1.7
1.6
1.5
1.4
1.3
1.2
1.1
1.0
0.9
0.8
0.7
0.6
0.5
0.4
0.3
0.2
0.1
0 0.1 0.2 0.3 0.4 0.5 0.6 0.7 0.8 0.9 1.0 1.1 1.2 1.3 1.4 1.5 1.6 1.7
E (e.v.)
0 0.05 0.1 0.2 0.3 0.4 0.5 0.6 0.7 0.8 0.9
SODIUM CONCENTRATION (x)

terms of the filling of a zone is only one possible explanation of the data. An equally plausible interpretation could be made in terms of an overlap in the band structure. A theoretical calculation of the band structure of sodium tungsten bronze might be able to establish whether or not either interpretation is reasonable. Such a calculation may prove to be quite feasible because of the high degree of symmetry of the bronzes.

VII. LITERATURE CITED

1. P. Debye, Ann. Physik, 39, 789 (1912)
2. M. Born and T. von Karman, Physik. Z., 13, 297 (1912)
3. B. W. Brown and E. Banks, J. Am. Chem. Soc., 76, 963 (1954)
4. G. Hagg, Nature, 135, 874 (1935)
5. E. O. Brimm, J. C. Brantly, J. H. Lorenz, and M. H. Jellinek, J. Am. Chem. Soc., 73, 5427 (1951)
6. B. W. Brown and E. Banks, Phys. Rev., 84, 609 (1951)
7. W. Gardner and G. C. Danielson, Phys. Rev., 93, 46 (1954)
8. F. Kupka and M. J. Sienko, J. Chem. Phys., 18, 1296 (1950)
9. P. M. Stubbin and D. P. Mellor, J. Proc. Roy. Soc. N. S. Wales, 82, 225 (1948)
10. C. Rosen, B. Post, and E. Banks, Acta Cryst., 9, 6 (1956)
11. P. Sidles, Electrical Resistivity of Sodium Tungsten Bronze, [Unpublished Research] Ames Laboratory of the U. S. Atomic Energy Commission, Ames, Iowa, 1957
12. J. F. Smith and G. C. Danielson, J. Chem. Phys., 22, 266 (1954)
13. J. F. Smith, Phys. Rev., 95, 1369 (1954)
14. A. Euken, "Handbuch der Experimental Physik", Vol. 8, p. 47, Akademische Verlagsgesellschaft M.B.H., Leipzig, 1929
15. W. H. Keesom and V. N. Van den Ende, Proc. Akad. Sci. Amsterdam, 33, 243 (1930)
16. W. H. Keesom and K. Clusius, Proc. Akad. Sci. Amsterdam, 35, 309 (1932)
17. J. A. Morrison, D. Patterson, and J. S. Dugdale, Can. J. Chem., 33, 375 (1955)

18. F. J. Webb and J. Wilks, Proc. Roy. Soc. (London), A230, 549 (1955)

19. I. Estermann, Phys. Rev., 78, 83 (1950)

20. H. A. Fairbank and C. T. Lane, Rev. Sci. Instr., 18, 525 (1947)

21. W. F. Giauque, J. W. Stout, and C. W. Clark, J. Am. Chem. Soc., 60, 1053 (1938)

22. J. R. Clement and E. H. Quinnell, Rev. Sci. Instr., 23, 213 (1952)

23. H. F. Stimson, J. Research Nat. Bur. Standards, 42, 209 (1949)

24. H. van Dijk and D. Schoenberg, Nature, 164, 151 (1949)

25. H. van Dijk and M. Durieux, A pressure-temperature relation for liquid helium. [Unpublished calculation] Kamerlingh Ohnes Laboratorium der Rijksuniversiteit, Neiuwsteeg 18, Leiden, Nederland, 1955

26. J. R. Clement*, J. K. Logan, and J. Gaffney, Phys. Rev., 100, 743 (1955)

27. M. Born and K. Huang, "Dynamical Theory of Crystal Lattices", Oxford, London, 1954

28. A. H. Wilson, "The Theory of Metals", 2nd ed., p. 135, Cambridge, London, 1953

29. A. Sommerfeld and N. H. Frank, Revs. Mod. Phys. 3, 1 (1931)

30. C. Kittel, "Introduction to Solid State Physics", p. 230, Wiley, New York, 1953

31. F. Seitz, " The Modern Theory of Solids", p. 140, McGraw-Hill, New York, 1940

32. D. R. Hartree, Proc. Cambridge Phil Soc., 24, 89 (1928)

33. V. Fock, Z. Physik, 61, 126 (1930)

---

*In particular, see the note added in proof at the end of this article.

34. H. Koppe, Z. Naturforsch., 2a, 429 (1947)

35. E. P. Wohlfarth, Phil. Mag., 41, 534 (1950)

36. E. P. Wigner, Trans. Faraday Soc., 34, 678 (1938)

37. M. J. Buckingham and M. R. Scharforth, Proc. Phys. Soc. (London), A67, 828 (1954)

38. D. Bohm and D. Pines, Phys. Rev., 82, 625 (1951)

39. D. Pines and D. Bohm, Phys. Rev., 85, 338 (1952)

40. D. Bohm and D. Pines, Phys. Rev., 92, 609 (1953)

41. D. Pines, Phys. Rev., 92, 626 (1953)

42. M. E. Straumanis, J. Am. Chem. Soc., 71, 679 (1949)

43. J. B. Nelson and D. P. Riley, Proc. Phys. Soc. (London), 57, 160 (1945)

44. H. J. Hoge, Rev. Sci. Instr., 20, 59 (1949)

45. F. E. Terman, "Radio Engineers' Handbook", p. 215, McGraw-Hill, New York, 1943

46. M. P. Garfunkel and A. Wexler, Rev. Sci. Instr., 25, 170 (1954)

47. H. S. Sommers, Rev. Sci. Instr., 25, 793 (1954)

48. W. Cawood and H. S. Patterson, Trans. Faraday Soc., 29, 514 (1933)

49. J. R. Reitz, Methods of the one-electron theory of solids. In Seitz, F. and Turnbull, D., eds., "Solid State Physics", Vol. 1, p. 24, Academic Press, New York, 1955

50. D. Pines, Electron interaction in metals. In Seitz, F. and Turnbull, D., eds., "Solid State Physics", Vol. 1, p. 400, Academic Press, New York, 1955

VIII. ACKNOWLEDGMENTS

The author wishes to express his appreciation to Dr. J. F. Smith for his guidance and advice in this research. Special thanks are extended to Dr. M. Griffel for introducing the author to the field of cryogenics. The author wishes to acknowledge the benefit of discussions with Dr. L. D. Jennings and Dr. C. A. Swenson on experimental techniques and interpretation of the data. The author also wishes to thank Miss Judith Kingston for assistance in some of the calculations and Mr. John Greiner for assistance in some of the measurements.